Chapter 3
Automotive Body Structural Elements

A unique characteristic of automobile body structure is the use of thin-walled structural elements. If a typical structural element from civil engineering—an I beam—is compared to a typical element from an automobile structure—a rocker beam—the difference in section proportions becomes apparent, Figure 3.1. If we compare the proportion of each section, the width to the thickness ratio, we see that it is relatively large for the automobile section. Further, we see that, unlike the I beam, the auto section is non-symmetrical, and that it is a fabrication of several formed pieces spot welded together. All of these differences lead to important differences in physical behavior, which we will cover in this chapter.

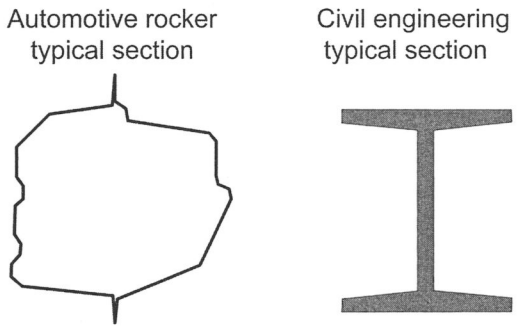

Figure 3.1 Beam sections.

3.1 Overview of Classical Beam Behavior

As a foundation for automotive beam behavior, we begin with classical beam behavior. This behavior is best embodied in a long straight beam with an I beam section; our assumptions are that the section is symmetric, the applied forces are down the axis of symmetry for the section, the section will not change shape upon loading, the deformation of the beam will be in the plane and in the direction of the applied load, the internal beam stresses vary in direct proportion with the strain, and failure is defined as yielding of the outermost fiber.

3.1.1 Static equilibrium at a beam section

The behavior of a beam under loading depends on the resulting bending moments at sections along the beam. To determine these moments, we can imagine the beam, Figure 3.2a, cut at some distance x from the end, Figure 3.2b. Looking at the left portion of the beam, an upward shear load, V, and a counter clockwise bending moment, M, act on the cut section. By setting the beam portion into static equilibrium we can find both $V(x)$ and $M(x)$. These are related by, Figure 3.2c, or the bending moment at a location x is equal to the area under the shear diagram between 0 and x.

$$M(x) = \int_0^x V dx \tag{3.1}$$

where:

$M(x)$ = Bending moment on a section at x

V = Shear load on section at x

x = Coordinate along length of beam

In Equation 3.1 and subsequent equations where the bending moment, $M(x)$, appears, a positive bending moment is defined to be one which bends the beam such that the radius of curvature is above the beam.

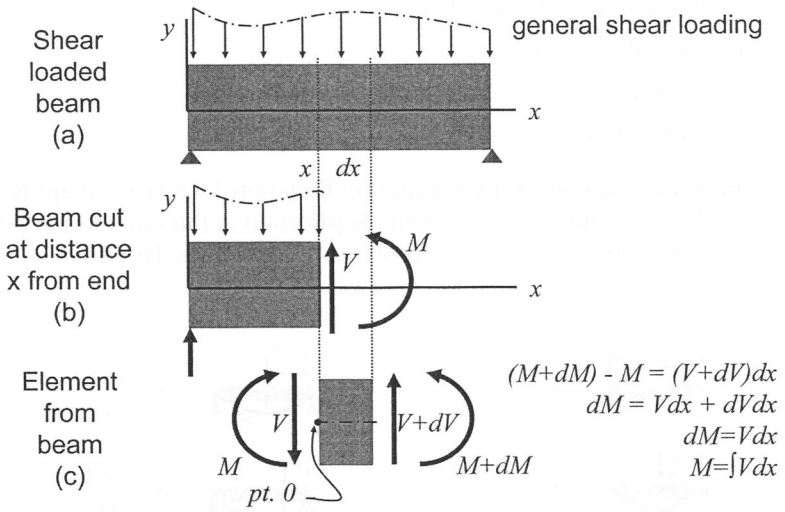

Figure 3.2 Beam equilibrium.

3.1.2 Stress over a beam section

At any cut of a beam, the direct stress varies linearly with the distance from the neutral axis, z, according to

$$\sigma = -\frac{Mz}{I} \tag{3.2}$$

where:

z = vertical distance from point of interest to the section neutral axis. (Defined to be positive in the upward direction.)

$M(x)$ = Bending moment on the section

σ = Direct stress at point of interest

The *moment of inertia*, I, is given by:

$$I = \int_{SECTION} z^2 dA \tag{3.3}$$

3.1.3 Beam deflection

The deflected shape of a beam may be described by a function, $y = f(x)$, where y is the lateral deflection from the initial shape at a distance x from the end. The curvature of the deflected beam at the distance x can be approximated by the second derivative, y''. This curvature is directly proportional to the bending moment acting at that section:

$$y'' = \frac{M(x)}{EI} \tag{3.4}$$

where:

$M(x)$ = Bending moment on a section at x

y'' = Curvature of the beam at x

E = Young's modulus

I = Moment of inertia

The deflection of a beam results by integrating Equation 3.3 twice and applying specific boundary conditions for the beam. Application of this equation provides useful results for stiffness for several typical beam conditions, Figure 3.3.

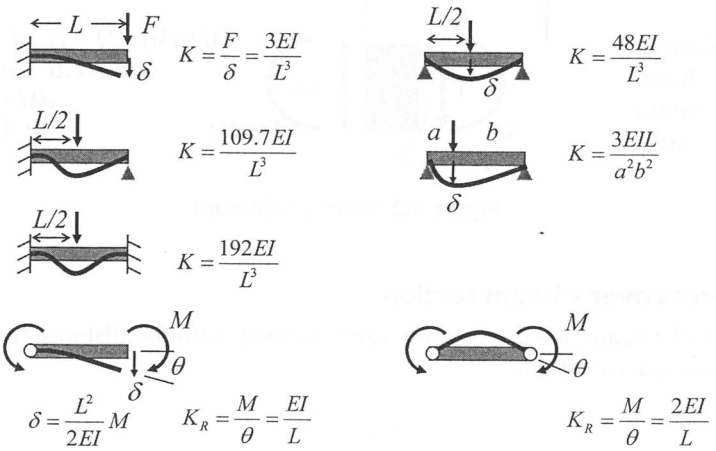

Figure 3.3 Beam stiffness equations.

Example: Cross member beam

The front motor compartment cross member holds the hood latch, Figure 3.4. Under use, aerodynamic loading places a vertical load of *1000 N* at the center of this beam. We wish to have no yielding (σ_y=*210 N/mm²*) in the cross member under this load, and a maximum linear deflection at the hood latch of *3 mm*. The size of the steel section is given as *30 mm* square with a thickness of *t=1.0 mm* and length *1000 mm*. We need to find if this section size will meet both the above requirements.

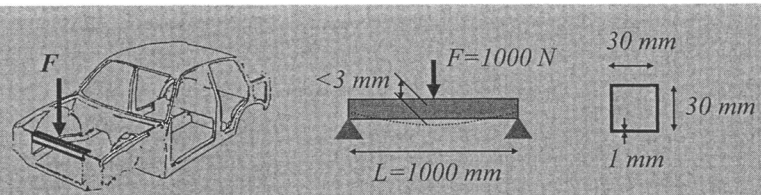

Requirements:
Stress less than $\sigma_{DESIGN}=210\ N/mm^2$
Deflection less than $3\ mm$

Figure 3.4 Motor compartment cross member.

The cross member may be modeled as a simply supported beam (in which the end restraints only prevent deflection at the ends and do not apply moments). We can take an arbitrary cut at x units from the end and between the left end and the center, Figure 3.5a. At this cut a shear force, V, acts and we place the left side of the beam into equilibrium to determine the value of V.

$$\begin{aligned} -500 + V &= 0 \\ V &= 500N \end{aligned} \quad \text{for } 0<x<L/2$$

Similarly, for a cut between the center and right end:

$$\begin{aligned} -500 + 1000 + V &= 0 \\ V &= -500N \end{aligned} \quad \text{for } L/2<x<0$$

The value for V is plotted as the shear diagram, Figure 3.5b. Taking the area under this curve up to position x and using Equation 3.1, the moment diagram results, Figure 3.5b. The maximum bending moment is at $x=L/2$ and is

$$M(L/2) = \int_0^{L/2} V dx = (500N)(1000mm/2) = 250000Nmm$$

Examining Equation 3.2 for stress, we see the maximum stress occurs along the length of the beam where bending moment is maximum, and at a point on the section which farthest from the neutral axis, $z = \pm 15\ mm$.

Calculating the moment of inertia, I, as shown in Figure 3.5c:

For the two side walls, the moment of inertia is

$$I_1 = I_2 = \frac{tb^3}{12} = \frac{(1mm)(30mm)^3}{12} = 2250mm^4$$

For the top or bottom wall, the moment of inertia is the inertia about the center of area for that wall plus the transfer inertia—the area of the wall times the square of the distance from the section's neutral axis:

$$I_3 = I_4 = \frac{wt^3}{12} + wt\left(\frac{b}{2}\right)^2 \cong (30mm)(1mm)\left(\frac{30mm}{2}\right)^2 = 6750mm^4$$

Where we have neglected the first term, as it is very small for thin-walled sections where t is small relative to w or b. The total section moment of inertia is,

$$I = I_1 + I_2 + I_3 + I_4 = 2(2250 + 6750)mm^4 = 18{,}000mm^4$$

Substituting values into Equation 3.2

$$\sigma = -\frac{Mz}{I} = \frac{250{,}000 N/mm(\pm 15 mm)}{18000 mm^4} = \pm 208 N/mm^2$$

where the tensile stress (+) is at the lower cap *(z=–15 mm)* and the compressive stress (–) is at the upper cap *(z=15 mm)*.

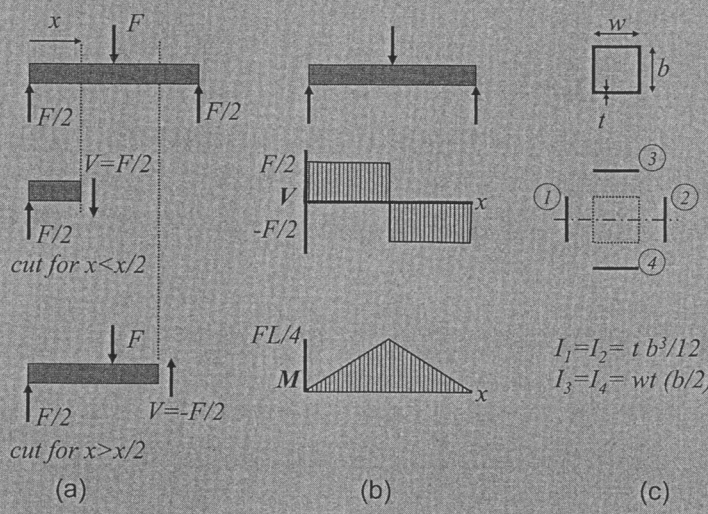

Figure 3.5 Cross member as simple beam.

Now looking at the deflection at the center of the span, we can use a result of Equation 3.4 contained in Figure 3.3:

$$k = \frac{applied\ load}{deflection} = \frac{48EI}{L^3}$$

$$deflection = \frac{L^3}{48EI}(applied\ load)$$

$$deflection = \frac{(1000 mm)^3}{48(207000 N/mm^2)(18000 mm^4)}(1000 N) = 5.6 mm$$

So for this example, the strength requirement is met *(208 N/mm² < 210 N/mm²)*, but the deflection requirement is not *(5.6 mm>3 mm)*. The section size or thickness must be increased to satisfy the deflection requirement.

Note that the assumptions of the classical equations are met, as the beam is symmetrical and symmetrically loaded. Also, due to its thick-walled section proportions, the beam failure mode is by yield.

With this summary of classical beam results, we can now look at the unique behavior of automotive structural elements. In this discussion of body structural elements, we will divide them into two general types: 1) frameworks constructed of beams, and 2) panels, Figure 3.6. In the next section we will develop tools to understand the unique behavior of automotive beams.

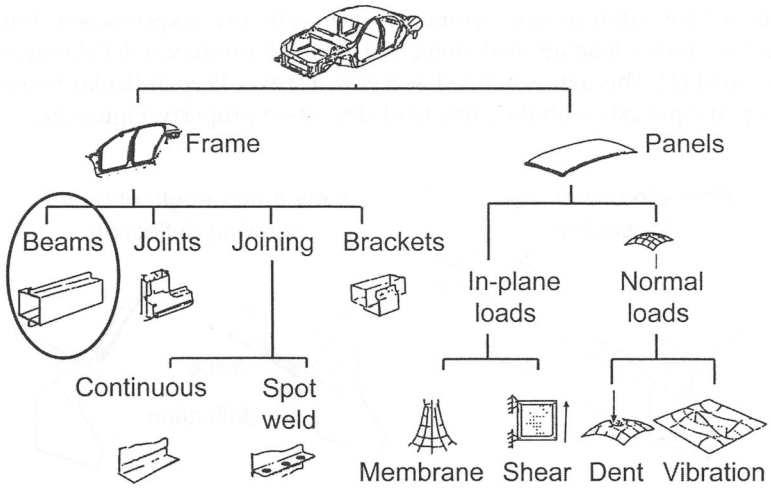

Figure 3.6 Structural element classification.

3.2 Design of Automotive Beam Sections

Several characteristics of automotive beams require analytical tools beyond classical beam theory. Below we will treat 1) the non-symmetrical nature of automotive beams, 2) local distortion of the section at the point of loading, 3) twisting of thin-walled members, 4) the effect of spot welds on structural performance.

3.2.1 Bending of non-symmetric beams

Beam sections in automotive applications are typically non-symmetrical, and we must develop the ability to predict deflection and stress for these sections. A symmetrically loaded section will deflect in the same direction as the applied load, Figure 3.7a. The deflection of a beam with a non-symmetrical section in general will not be colinear with the applied load, Figure 3.7b.

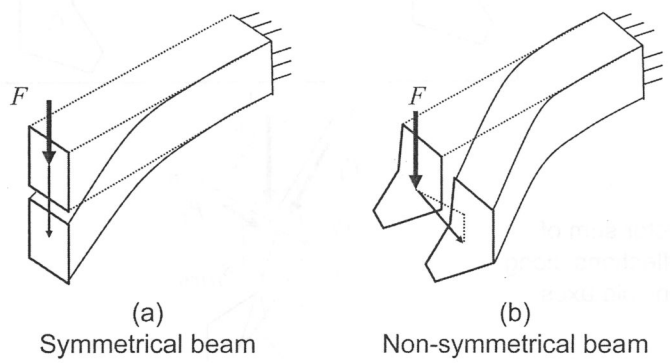

Figure 3.7 Deflection of symmetrical and non-symmetrical beams.

However, for any arbitrary non-symmetric section there is a specific axis through its centroid for which a load applied along that axis will produce a deflection colinear with that load [1]. This axis is defined as a *principle axis*. Perpendicular to this axis is a second principle axis with the same load-deflection property, Figure 3.8.

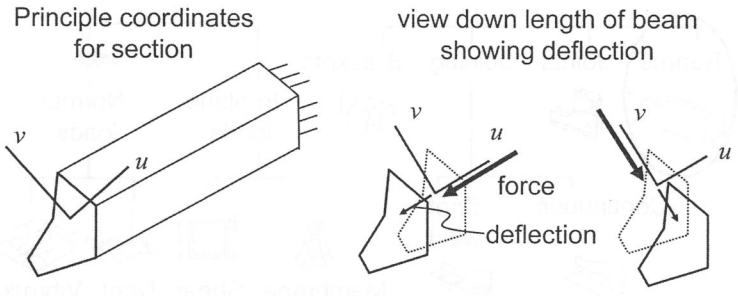

Figure 3.8 Non-symmetrical beam principle axes.

This suggests a way to predict deflections in a beam with a non-symmetric section and loaded in some arbitrary direction, Figure 3.9:

1. Resolve the load into components along each principle axis.
2. Solve for the resulting deflection for each of these components using the equations of Figure 3.3. Note that the moment of inertia is taken about the axis perpendicular to the load. Each of these deflections will be along the respective principle axis.
3. Take the vector sum of the two deflections to determine the magnitude and direction of the total deflection.

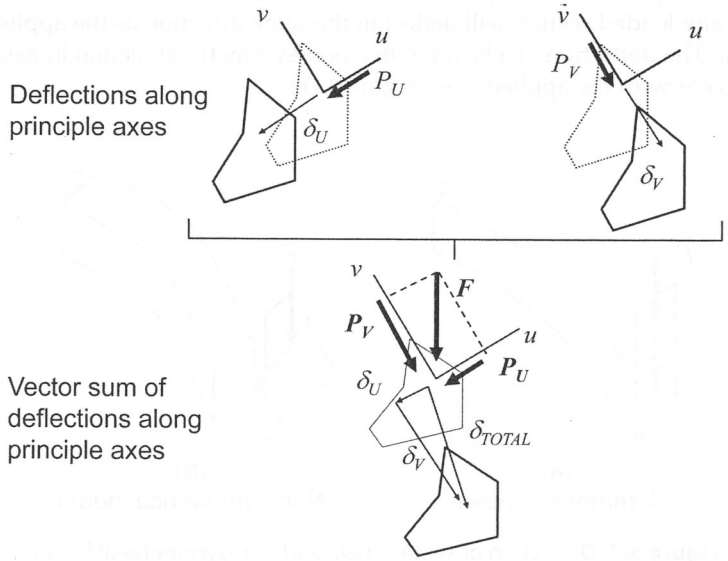

Figure 3.9 Non-symmetrical beam deflection.

For stress, the steps are similar after determining the bending moment vector acting on the section, Figure 3.10:

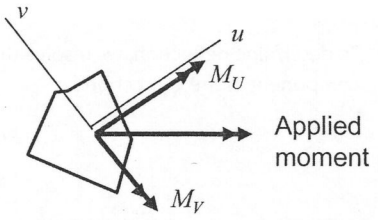

Figure 3.10 Moments acting on non-symmetrical beam.

1. Resolve the moment into components along each principle axis.
2. For each component of the moment, solve for the resulting stress using Equation 3.2. Note that the dimension z is the distance to the point of interest from the axis which is colinear with the moment vector, and the moment of inertia is about the same axis.
3. Take the algebraic sum of the two stresses for the resultant stress.

Example: Non-symmetric beam

Consider the steering column mounting beam, Figure 3.11. We can view this beam with non-symmetrical section as a cantilever with a downward vertical tip load, Figure 3.12a, and we are interested in determining the tip deflection and also the stress at a specific point *A* where the beam joins the restraining structure.

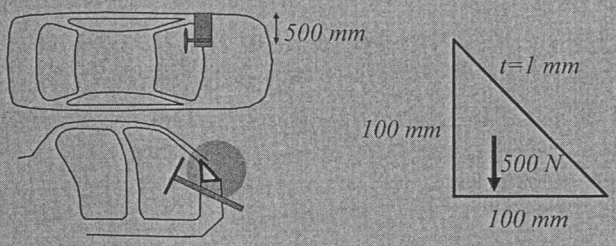

Figure 3.11 Steering column support beam.

The section properties can be determined using section analysis software [2], with the resulting orientation of the two principle axes shown along with the moments of inertia about these axes, Figure 3.12b.

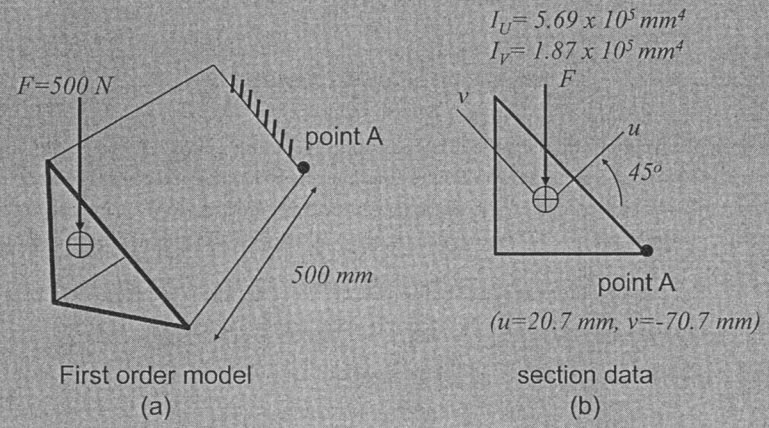

Figure 3.12 Section principle axes.

To determine deflection, we resolve the applied load into a component in the *u* direction and a component in the *v* direction.

$$F_V = F\cos(\theta) = 500\cos(45^o) = 353.5N$$
$$F_U = F\sin(\theta) = 500\sin(45^o) = 353.5N$$

Then we can use the cantilever equation from Figure 3.3 to determine the deflections along each of these axes, Figure 3.13.

$$\delta_U = \frac{F_U L^3}{3EI_V}, \quad \delta_V = \frac{F_V L^3}{3EI_U}$$

$$\delta_U = \frac{500N(0.707)(500mm)^3}{3(207\ x10^3\ N/mm^2)(1.87\ x10^5\ mm^4)} = 0.38mm$$
$$\delta_V = \frac{500N(0.707)(500mm)^3}{3(207\ x10^3\ N/mm^2)(5.69\ x10^5\ mm^4)} = 0.125mm$$

Adding the deflection vectors yields the total deflection, Figure 3.13b.

$$\delta_{TOTAL} = \sqrt{\delta_U^2 + \delta_V^2} = 0.4mm$$

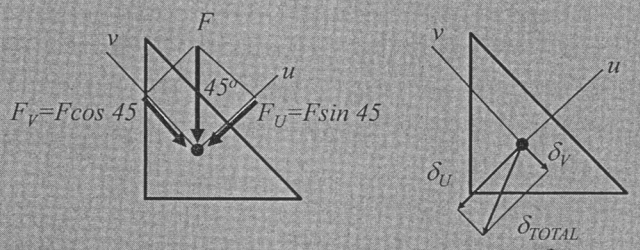

Force components in principle coordinate system (a)

Vector sum of deflections (b)

Figure 3.13 Beam deflection calculation.

To determine stress at point A, we first identify the bending moment at the section of interest. The bending moment for the section at the wall is a counterclockwise moment, and using the right-hand rule is a horizontal vector pointing to the right, Figure 3.14. Next, take the components of the applied bending moment along the *u* and *v* axes. We can see that the moment vector down the u axis would place the bending radius of curvature below the beam, and similarly for the moment along the v axis; this gives both moment components a negative sign, Figure 3.15. Solving for the stress from each of these moments using Equation 3.2 (The distance from the neutral axis to the point, z, is shown here as v and u.):

$$\sigma_U = -\frac{M_U v}{I_U}$$
$$\sigma_U = -\frac{(-500N \cdot 500mm \cdot \cos 45^o)(-70.7mm)}{5.69\ x10^5\ mm^4}$$
$$\sigma_U = -22N/mm^2$$

$$\sigma_V = -\frac{M_V u}{I_V}$$

$$\sigma_V = -\frac{(-500N \cdot 500mm \cdot \sin 45^o)(20.7mm)}{1.87x10^5 mm^4}$$

$$\sigma_V = +19.57N/mm^2$$

$$\sigma_{POINT\ A} = \sigma_U + \sigma_V$$

$$\sigma_{POINT\ A} = (-22 + 19.57)N/mm^2$$

$$\sigma_{POINT\ A} = (-22.43)N/mm^2$$

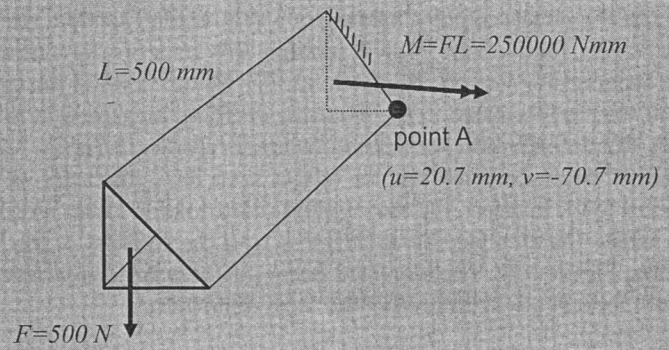

Figure 3.14 Moment vector.

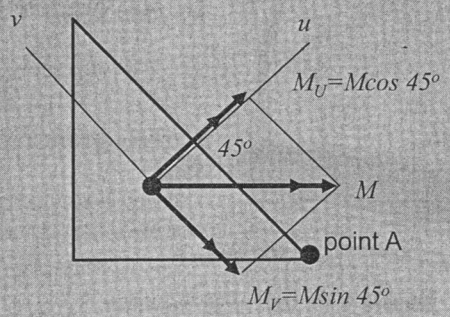

Figure 3.15 Moment resolved into principle components.

3.2.2 Point loading of thin-walled sections

In the development of beam theory for thin-walled sections, we have assumed that the applied point loads only influence the beam through the resulting bending moments. In practice, with thin-walled sections the point load also distorts the beam section in the vicinity of the load, Figure 3.16. This undesirable distortion leads to a reduced apparent beam stiffness and increased local stress. In this section, we will develop tools to predict the degree of local distortion and strategies to minimize local distortion.

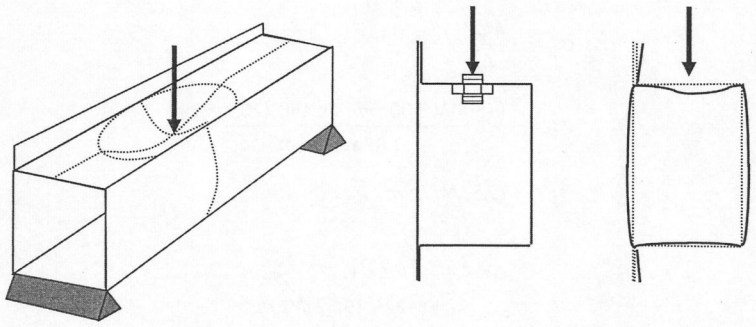

Figure 3.16 Local deformation under point load.

To investigate the effects of point loading of a thin-walled section, consider the latch structure of a van, Figure 3.17. We will idealize this structure as a simply supported beam with rectangular section. The latch applies a point load at the center of the section, and we are interested in the resulting stiffness measured at this point. Under such a load, the deformation we would observe is shown in Figure 3.18. In addition to the idealized beam deformation, we would see a local distortion of the section near the point load. In effect, the thin-walled point-loaded beam would be two springs in series: the idealized beam stiffness, and the stiffness of the local distortion of the section, Figure 3.18. The idealized beam stiffness is summarized in Figure 3.3. Now we will look at a way to predict the local distortion.

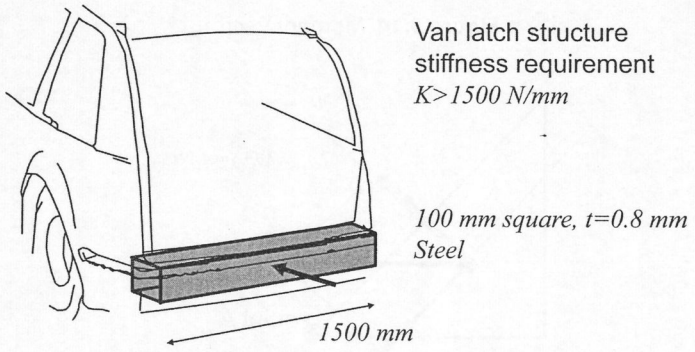

Figure 3.17 Van cross member.

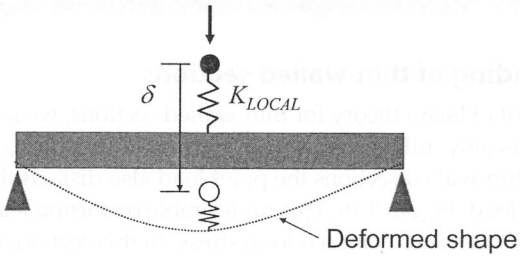

Figure 3.18 Deflection of van latch structure.

Looking again at the distorted beam, we can separate out the idealized beam deflection by imagining the beam supported along its neutral axis, Figure 3.19a. The point load is reacted by a deformed patch on the top surface of the beam which we denote as the *affected zone* (we take the length and width of the affected zone to be the section width, b). The affected zone can now be imagined to be cut into slices of unit length with each slice acting as a spring supporting the load. Figure 3.19b. As such, the distorted sections act as an *elastic foundation* for the point load.

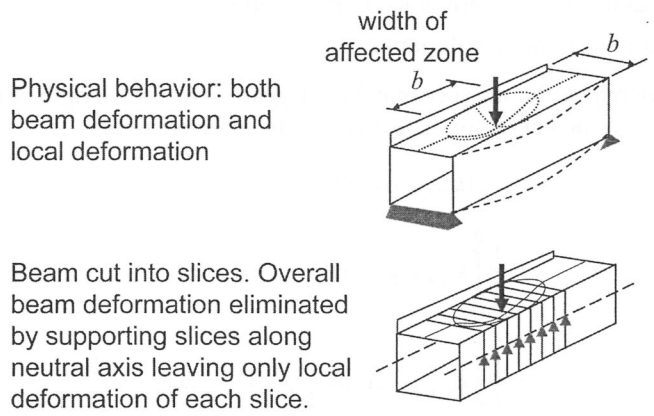

Figure 3.19a Idealized beam.

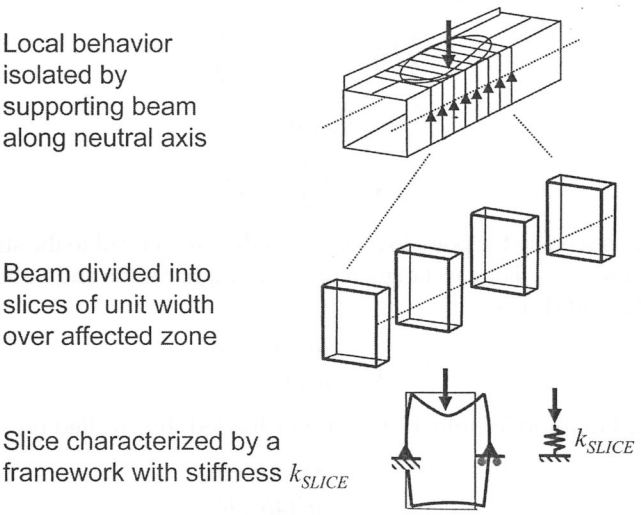

Figure 3.19b Idealized beam.

Consider the foundation stiffness to be k_{SLICE} *N/mm/mm* and assume the deflected shape for the top plate centerline is, Figure 3.20:

$$y = -\Delta \sin \frac{\pi x}{b}, \quad 0 < x < \pi$$

where:

y = Normal deflection of top plate at centerline

b = Plate width

Δ = Plate deflection at point of load application

x = Coordinate along length of plate

The strain energy, *de*, in one slice may be integrated over the length of the affected zone to arrive at the energy of distortion for the affected zone:

$$de = \frac{1}{2}(k_{SLICE}\, dx)(y)^2$$

$$e = \frac{1}{2}\int_0^b k_{SLICE}(y)^2 dx$$

$$e = \frac{1}{2}\int_0^b k_{SLICE}(-\Delta \sin \frac{\pi x}{b})^2 dx = \frac{1}{2} k_{SLICE}\Delta^2 \frac{b}{2}$$

We can equate this distortion energy, *e*, to the work done by the external force, *1/2FΔ*. Equating work to strain energy yields:

$$\frac{1}{2}F\Delta = \frac{1}{2}k_{SLICE}\Delta^2 \frac{b}{2}$$

$$\frac{F}{\Delta} = \frac{1}{2}k_{SLICE}b$$

$$K_{LOCAL} = \frac{1}{2}k_{SLICE}b \tag{3.5}$$

So the stiffness as seen by the point load, k_{LOCAL}, is directly related to the stiffness of a slice of the section, k_{SLICE}. For a rectangular section h high, b wide and t thick, Figure 3.21, the stiffness of a unit slice is:

$$k_{SLICE} = \frac{16Et^3(h+b)}{b^3(4h+b)} \tag{3.6}$$

so substituting Equation 3.6 into 3.5 for a point-loaded thin-walled rectangular beam:

$$K_{LOCAL} = \frac{8Et^3(h+b)}{b^2(4h+b)}$$

where:

K_{LOCAL} = Local stiffness of section under a central point load

t = Section thickness

h = Section height

b = Section width

E = Young's Modulus

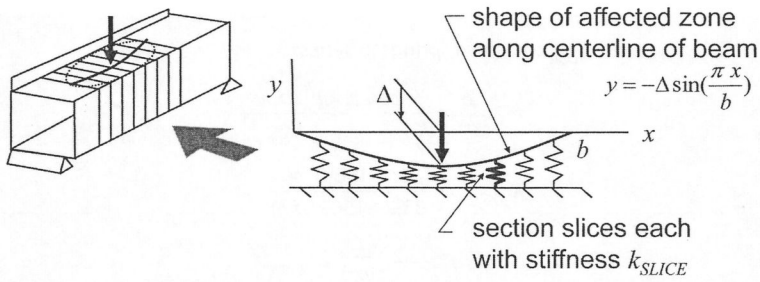

$$\left[\begin{array}{l}\text{Energy stored by local stiffness}\\ \text{at point of load application}\end{array}\right] = \left[\begin{array}{l}\text{Energy stored by distortion}\\ \text{of all section slices}\end{array}\right]$$

Figure 3.20 Idealized beam analysis.

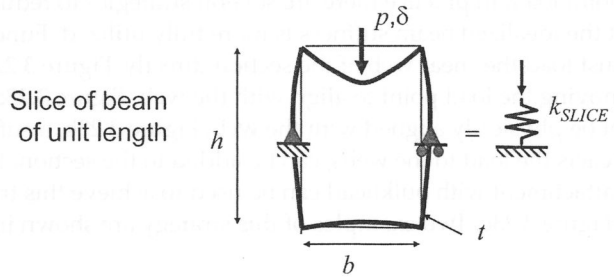

Figure 3.21 Rectangular section under point load.

Example: Local deformation

As a numerical example, consider the van cross member of Figure 3.17. Looking first at the idealized beam deflection and using the stiffness equations of Figure 3.3:

$$K_{IDEAL\ BEAM} = \frac{48EI}{L^3}$$

$$K_{IDEAL\ BEAM} = \frac{48(207000\frac{N}{mm^2})(5.33x10^5 mm^4)}{(1500mm)^3}$$

$$K_{IDEAL\ BEAM} = 1569\frac{N}{mm}$$

For the dimensions given, the local stiffness is:

$$K_{LOCAL} = \frac{8Et^3(h+b)}{b^2(4h+b)} = \frac{8(207000\frac{N}{mm^2})(0.8mm)^3(100mm+100mm)}{(100mm)^2(4\cdot 100mm+100mm)}$$

$$K_{LOCAL} = 33.9\frac{N}{mm}$$

Now consider $K_{IDEAL\ BEAM}$ and K_{LOCAL} to be two springs in series:

$$K_{SYSTEM} = \frac{K_{IDEAL\ BEAM} K_{LOCAL}}{K_{IDEAL\ BEAM} + K_{LOCAL}}$$

$$K_{SYSTEM} = \frac{(33.9)(1569)}{33.9 + 1569} \frac{N}{mm}$$

$$K_{SYSTEM} = 33.2 \frac{N}{mm}$$

So, because of local distortion, the stiffness at the point of load application is only 2% of the idealized beam stiffness. The large beam section is not being effectively used.

The above example demonstrates why an untreated thin-walled section performs so poorly under a point load. In practice there are several strategies to reduce this local distortion so that the idealized beam stiffness is more fully utilized. Fundamentally the point load must load the shear web of the section directly, Figure 3.22. This can be achieved by moving the load point to align with the web, Figure 3.23a. When the load point cannot be physically aligned with the web, Figure 3.23b, a stiff structural element, which reacts the load to the webs, can be added to the section. Finally, a through-section attachment with bulkhead can be used to achieve this transfer of load to the web, Figure 3.23c. Two examples of this strategy are shown in Figure 3.24.

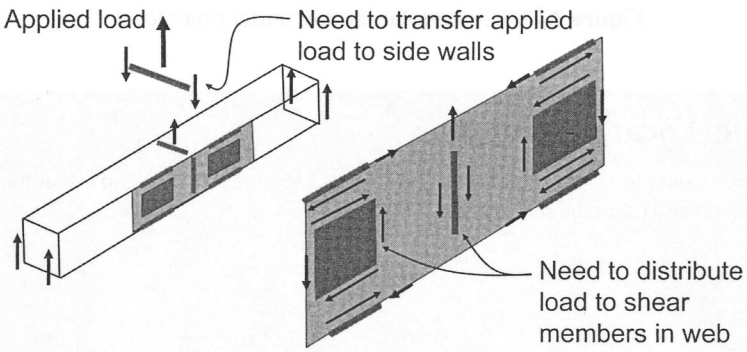

Figure 3.22 Shear web.

3.3 Torsion of Thin-Wall Members

Elementary treatment of twisting of bars is limited to solid circular sections. For solid circular bar, the basic equations [3] for angular deflection and for shear stress are given by:

$$\theta = \frac{TL}{GJ} \tag{3.7a}$$

$$\tau = \frac{Tr}{J} \tag{3.7b}$$

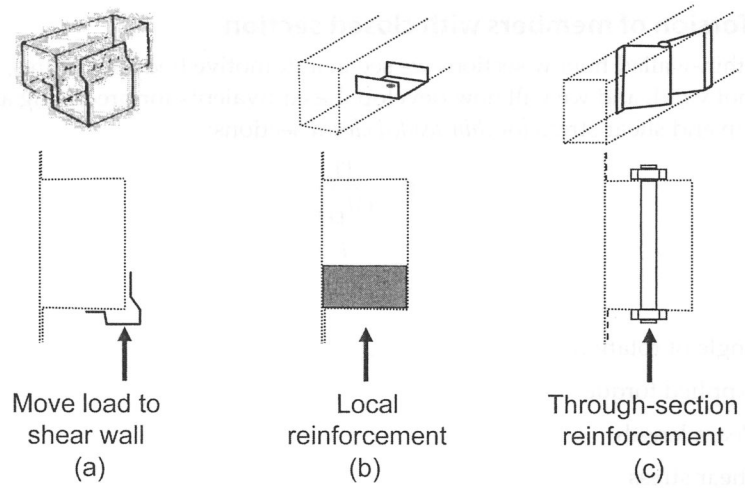

Figure 3.23 Loading the shear web.

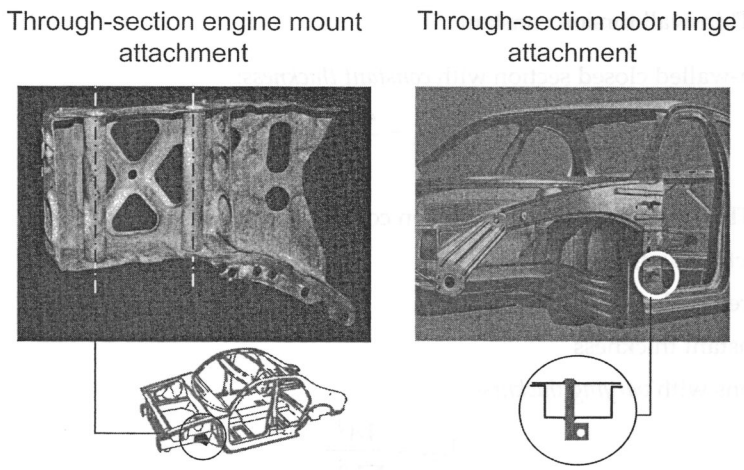

Figure 3.24 Example sections reacting a point load. (Courtesy of A2Mac1.com Automotive Benchmarking, and the American Iron and Steel Institute, UltraLight Steel Auto Body

where:

T = Applied torque

θ = Resulting angle of twist

J = Polar moment of inertia

G = Shear modulus

L = Length of the bar

r = Radius of the bar

τ = Maximum shear stress (at the surface of the bar)

3.3.1 Torsion of members with closed section

For the thin-walled hollow sections we see in automotive body structures, Equations 3.7 are not valid, and we will now develop the equivalents for predicting angular deflection and shear stress for *thin-walled closed* sections:

$$\theta = \frac{TL}{GJ_{EFF}} \tag{3.8a}$$

$$\tau = \frac{T}{2At} \tag{3.8b}$$

where:

θ = angle of rotation

T = Applied torque

L = Beam length

τ = Shear stress

A = Area enclosed by the section

t = Thickness

J_{EFF} = Thin-wall torsion constant

For a thin-walled closed section with *constant thickness*:

$$J_{EFF} = \frac{4A^2t}{S} \tag{3.9}$$

where:

J_{EFF} = Thin-wall closed-section torsion constant with constant thickness

S = Section perimeter.

A = Area enclosed by the section

t = constant thickness

For sections with *varying thickness*:

$$J_{EFF} = \frac{4A^2}{\sum_i \frac{s_i}{t_i}} \tag{3.10}$$

where the section is divided into i segments each of uniform thickness, t_i, and length s_i.

We will now develop these equations [4]. Consider a thin-walled closed tube of arbitrary cross-section shape and length, L, Figure 3.25a. We apply equal and opposite torques at the ends of the tube and imagine the tube cut along its length, Figure 3.25b. All along one of the cut edges will be a shearing stress, τ_1, and we can look at the static equilibrium of a rectangular element adjacent to the cut, Figure 3.26a. Setting longitudinal forces into equilibrium gives $\tau_1 t_1 = \tau_2 t_2$. The quantity (τt) is the shearing force per unit length and we define this as *shear flow*, q. Further, setting moments on this element into equilibrium, Figure 3.26b, yields $q' = q$, or the shear flow on all sides of this element are equal. This shows that the shear flow, (τt), is uniform throughout the tube. Now we seek a relationship between shear flow and applied torque.

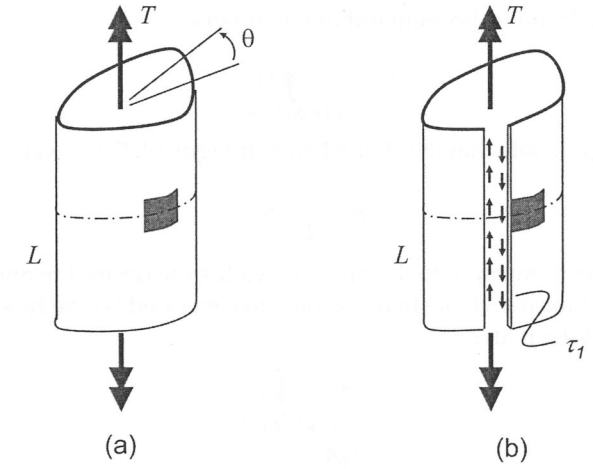

Figure 3.25 Thin-walled closed tube.

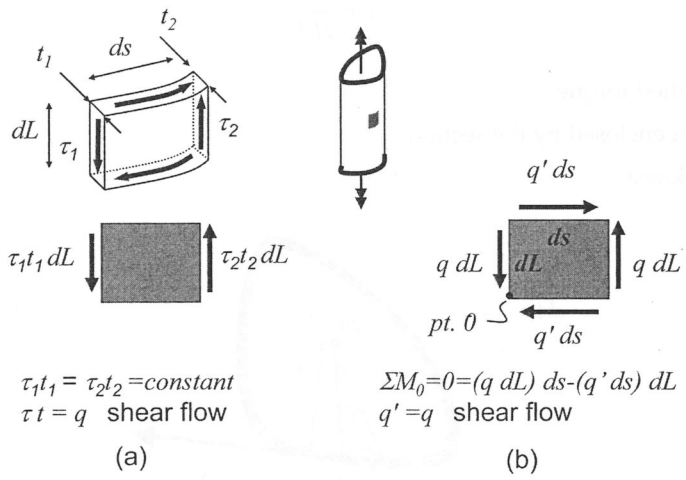

Figure 3.26 Element under torsion.

Looking at the end view of the tube, we can consider a small element of perimeter, dS. As shear flow is uniform throughout the tube, the force, dF, acting on this element is $dF=qdS$. This force is directed tangent to the section, and results in a small torque, dT, about some arbitrary point O contained within the interior of the section. The torque is equal to the force, dF, times the distance, r, from the line of action of the force to the point O, or $dT=rdF=rqdS$. To determine the total torque we must integrate around the perimeter:

$$T = \oint_{PERIMETER} rqdS$$

Since q is constant, it can be brought out of the integral:

$$T = q \oint_{PERIMETER} r dS$$

To solve this integral, note that the shaded area in Figure 3.27 is given by:

$$dA = \frac{1}{2} r dS$$

Substituting this relationship into the previous yields the desired relationship between stress and torque. (Note that A is the area enclosed by the tube perimeter and not the area of the material.):

$$T = 2q \oint_{PERIMETER} dA$$

$$T = 2qA$$

$$q = \frac{T}{2A}$$

$$\tau = \frac{T}{2tA} \tag{3.11}$$

where:

T = Applied torque

A = Area enclosed by the section

t = Thickness

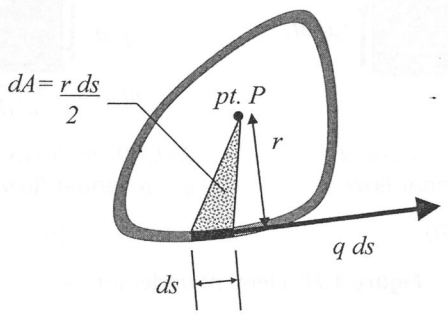

Figure 3.27 Tube section.

Now consider the angle of twist, θ, resulting from the application of the torque, T, Figure 3.25. We will equate the work done by the external torque to the strain energy stored within the twisted tube.

$$\text{external work from applied torque} = \frac{1}{2} T\theta$$

$$\text{strain energy} = \int \frac{1}{2} \gamma \tau dV = \int \frac{1}{2} \frac{\tau}{G} \tau dV = \int \frac{1}{2} \frac{\tau^2}{G} dV$$

$$\text{strain energy} = \iint \frac{1}{2} \frac{\tau^2}{G} t \, dL \, dS$$

using Equation 3.8 to substitute for shear stress, τ:

$$\text{strain energy} = \iint \frac{1}{2G}\left(\frac{T}{2At}\right)^2 t\, dL\, dS$$

$$\text{strain energy} = \frac{1}{2G}\frac{T^2}{(2A)^2}\iint \frac{1}{t}\, dL\, dS$$

$$\text{strain energy} = \frac{1}{2G}\frac{LT^2}{(2A)^2}\oint \frac{dS}{t}$$

Equating work to strain energy:

$$\frac{1}{2}T\theta = \frac{1}{2G}\frac{LT^2}{(2A)^2}\oint \frac{dS}{t}$$

$$\theta = \frac{TL}{4GA^2}\oint \frac{dS}{t}$$

Rearranging yields:

$$\theta = \frac{TL}{G\left[\dfrac{4A^2}{\oint \dfrac{dS}{t}}\right]} = \frac{TL}{GJ_{EFF}}, \qquad (3.12)$$

$$\text{where} \quad J_{EFF} = \frac{4A^2}{\oint \dfrac{dS}{t}}$$

which agrees with Equation 3.8a where the variables are defined. Note for the case where the thickness is constant, the effective torsional constant is

$$J_{EFF} = \frac{4A^2 t}{S} \qquad (3.13)$$

Example: Torsion of beam with closed section

Consider again the steering column mounting beam, Figure 3.28 but now under torsional loading. We are interested in the angle of rotation and the shear stress under a pure torque of $T=25x10^4\ Nmm$.

Equation 3.13 gives the effective torsion constant:

$$J_{EFF} = \frac{4A^2}{\oint \dfrac{dS}{t}} = \frac{4tA^2}{S} = \frac{4(1mm)\left(\frac{1}{2}(100mm)(100mm)\right)^2}{(100mm+100mm+141.4mm)} = 2.929x10^5 mm^4$$

Equation 3.12 results in the angle of twist:

$$\theta = \frac{TL}{GJ_{EFF}} = \frac{(25x10^4\ Nmm)(500mm)}{(78x10^3 N/mm^2)(2.929x10^5 mm^4)} = 5.47x10^{-3}\ rad\ (0.312^o)$$

Finally, Equation 3.11 results in the shear stress:

$$\tau = \frac{T}{2tA} = \frac{(25x10^4\,Nmm)}{2(1mm)\left(\frac{1}{2}(100mm)(100mm)\right)} = 25N/mm^2$$

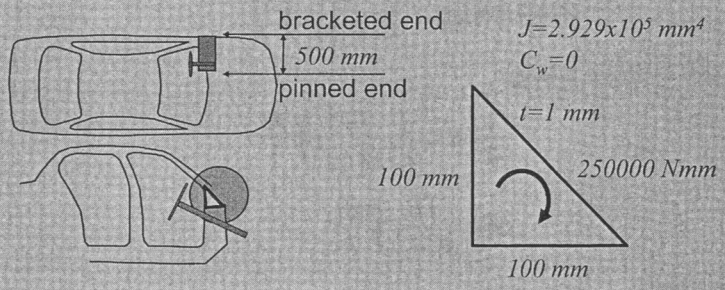

Figure 3.28 Steering column beam.

3.3.2 Torsion of members with open section

The above discussion concerned tubes with closed section. For open sections, the development of the equations requires application of the *theory of elasticity* and is beyond the scope of this book. However, we state the results [5] below, Figure 3.29, for a *thin-walled open* section of constant thickness:

$$J_{EFF} = \frac{1}{3}t^3S \tag{3.14a}$$

$$\tau = \frac{Tt}{J_{EFF}} \tag{3.14b}$$

where:

J_{EFF} = Torsion constant for an open section

S = Developed section length

t = Thickness

T = Applied torque

τ = Shear stress

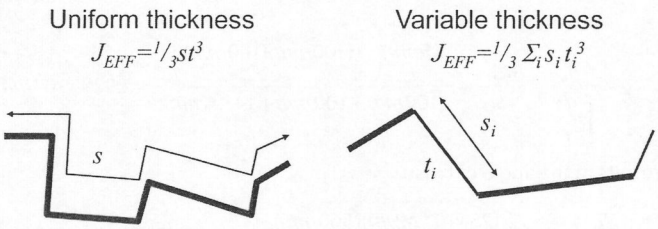

Figure 3.29 Torsion of open sections.

For open sections with non-uniform thickness:

$$J_{EFF} = \frac{1}{3}\sum_i t_i^3 S_i \tag{3.15}$$

where the section is divided into i segments each of uniform thickness, t_i, and length s_i.

Note the somewhat unexpected result that the shape of the open section does not enter the expressions, and in general open sections are much more flexible than a closed section of the same perimeter.

Example: Torsion of beam with open section

Consider again the steering column mounting beam as in the previous example, but now, rather than a closed section, there is a very thin slot as shown in Figure 3.30. Applying Equation 3.14a gives:

$$J_{EFF} = \frac{1}{3}t^3 S = \frac{1}{3}(1mm)^3(100mm + 100mm + 141.4mm) = 113.8mm^4$$

From Equation 3.8a:

$$\theta = \frac{TL}{GJ_{EFF}} = \frac{(25x10^4 Nmm)(500mm)}{(78x10^3 N/mm^2)(113.8mm^4)} = 14.1rad\ (803^o)$$

From Equation 3.14b:

$$\tau = \frac{Tt}{J_{EFF}} = \frac{(25x10^4 Nmm)(1mm)}{113.8mm^4} = 2197N/mm^2$$

Clearly both of these values are beyond the linearity assumptions; however, we learn that not only is the section *very* flexible, but the shear stress is quite high compared to the closed section of the previous example.

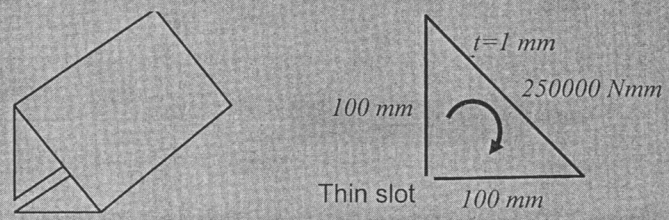

Figure 3.30 Slotted beam section.

3.3.3 Warping of open sections under torsion

The above examples for torsion of open and closed sections showed the open section to be relatively highly flexible. The reason open sections perform so poorly in torsion is that the section has considerable warping in the longitudinal direction, Figure 3.31. In Equations 3.14a and 3.14b, we assumed that this warping is unrestrained in any way. However, if we rigidly hold an end of the open tube and prevent warping, the stiffness of the tube can be markedly increased. In Figures 3.32 and 3.33, we provide formulae for prediction of angle of rotation when one or both ends of a tube are restrained from warping [6]. Note the use of the warping constant, *Cw*, for the section. Warping depends only on the geometry of the section,

with large *Cw* values indicating greater out-of-plane deformation, and *Cw=0* indicating the section remains planar under torque loading. For general sections, the constant *Cw* may be obtained using section analysis software, or for simple sections it may be calculated using the formulae shown in Figure 3.34 [6].

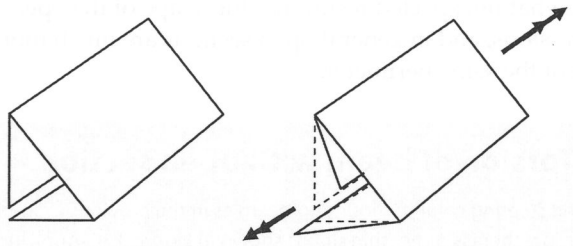

Figure 3.31 Open-section warping.

J=torsion constant, Cw=warping constant: $k=\sqrt{\frac{JG}{C_w E}}$

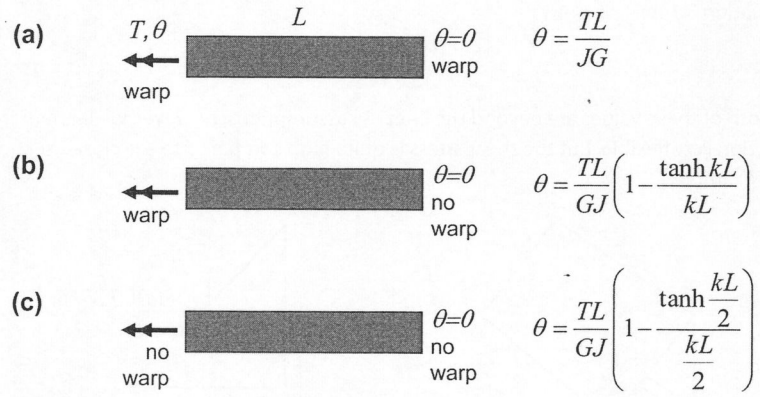

Figure 3.32 Formulae for twist of end-loaded warping tubes.

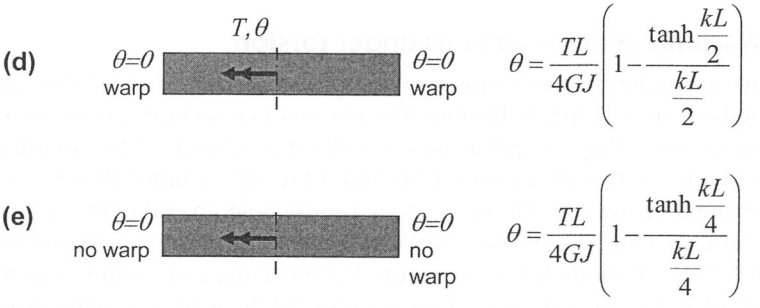

Figure 3.33 Formulae for twist of center-loaded warping tubes.

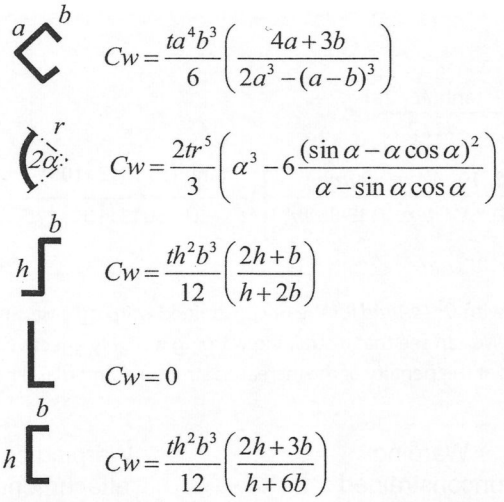

Figure 3.34 Formulae for warping coefficients.

Example: Warping beam

Look again at the steering column mounting beam with a very thin slot from the preceding example, Figure 3.30. Previously we allowed unrestrained warping in the calculation of angle of rotation, now we will constrain both ends from out-of-plane deflection by adding a very stiff mounting bracket to each end, Figure 3.35. Referring to Figure 3.32, the boundary conditions for this example match case *(c)*, and we use the relationship:

$$\theta = \frac{TL}{GJ}\left[1 - \frac{\tanh(kL/2)}{kL/2}\right]$$

where:

θ = Angle of twist with warping

T = Applied torque

G = Shear modulus

L = Beam length

J = Torsion Constant

$$k = \sqrt{\frac{JG}{C_w E}}$$

E = Young's Modulus

Cw = Warping constant

For this section, $J=113.8\ mm^4$ from the previous example, and we are given $CW=1.4x10^9\ mm^6$. Substituting into the above:

$$k = \sqrt{\frac{JG}{C_w E}} = \sqrt{\frac{(113.8mm^4)(78x10^3 N/mm^2)}{(1.4x10^9\ mm^6)(207x10^3 N/mm^2)}} =$$

$$k = 1.75013x10^{-4}\ /\ mm$$

and

$$\theta = \frac{TL}{GJ}\left[1 - \frac{\tanh(kL/2)}{kL/2}\right] =$$

$$\theta = \frac{25x10^4\,Nmm(500mm)}{(78x10^3\,N/mm^2)(113.8mm^4)}\left[1 - \frac{\tanh\left((1.75013x10^{-4}/mm)(500mm)/2\right)}{(1.75013x10^{-4}/mm)(500mm)/2}\right]$$

$$\theta = 8.98x10^{-3}\,rad$$

Compare this result with θ=*14.1 rad* for the unconstrained warping case, and θ=*5.47x10^{-3} rad* for the closed-section case. We can see that restraining warping is highly effective in stiffening an open tube. However, this comes at the penalty of the increased structure (and mass) needed to prevent warping, Figure 3.35.

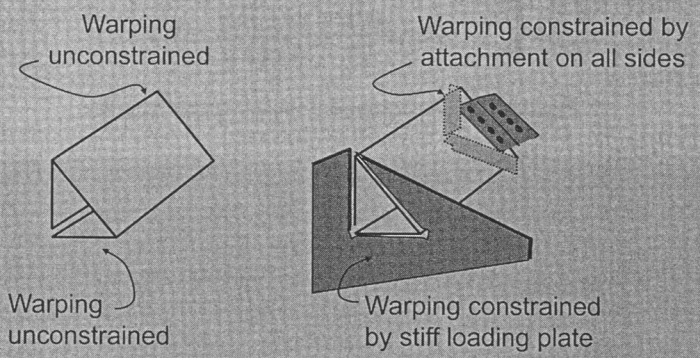

Figure 3.35 Constraining warping.

The physical means of restraining warping is often challenging to achieve in practice. In Figure 3.36, other boundary conditions are shown for the steering column beam for the cases (a), (b), (c) of Figure 3.32.

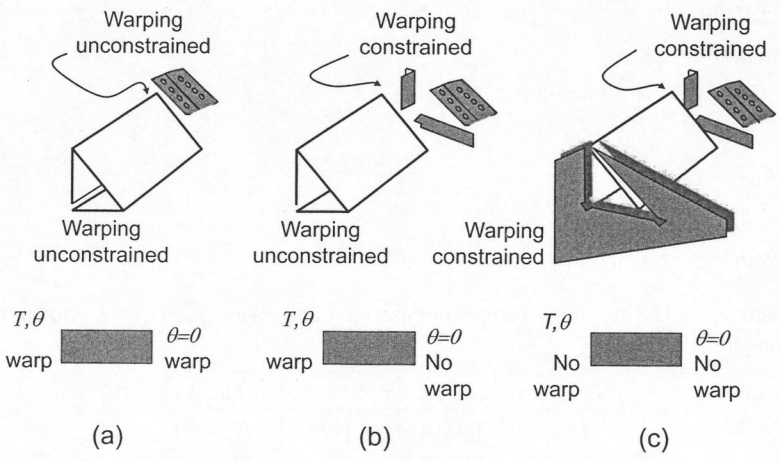

Figure 3.36 Constraining warping: Idealization.

Note that the effectiveness of restraining warping depends on the tube length; the stiffening influence of restraining warping diminishes as the tube becomes longer. Intuitively this is because the warping restraint primarily influences the region around tube end, and as the tube becomes longer this region becomes proportionately smaller.

Example: Effect of length of warping beam

As an example of the effect of beam length on angle of rotation, we continue with the example of the steering column mount tube and use the equations in Figure 3.32 to determine the angle of rotation for an open section tube with (a) unrestrained ends, (b) with one end restrained, (c) with two ends restrained, and a closed section (no warping). Figure 3.37 shows the resulting angle of rotation per unit length as we vary length from *400* to *1000 mm* for these cases. The trend of increasing angle of twist as length increases can be seen for cases (b) and (c) where we restrain warping. For the shorter tubes, *L=400 mm*, the both-ends-restrained open section, (c), is nearly as stiff (93%) as the closed section; for the longer tubes, *L=1000 mm*, the both-ends-restrained open section, (c), is only *15%* as stiff as the closed section.

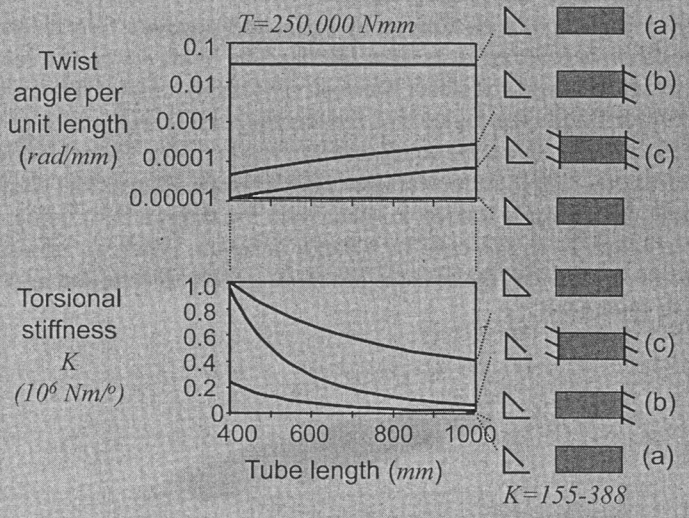

Figure 3.37 Twist angle: Varying length and end conditions.

3.3.4 Effect of spot welds on structural performance

Automotive body sections are fabrications of several formed elements, usually spot welded together. Spot welding is a robust and cost-efficient process for mass production, Figure 3.38, but does present some unique structural challenges. One of these is the addition of shear flexibility in the section which is most evident during torsion of fabricated sections. In this section we will develop tools to predict the degree of shear flexibility, the implications on section stiffness, and strategies to minimize the flexibility.

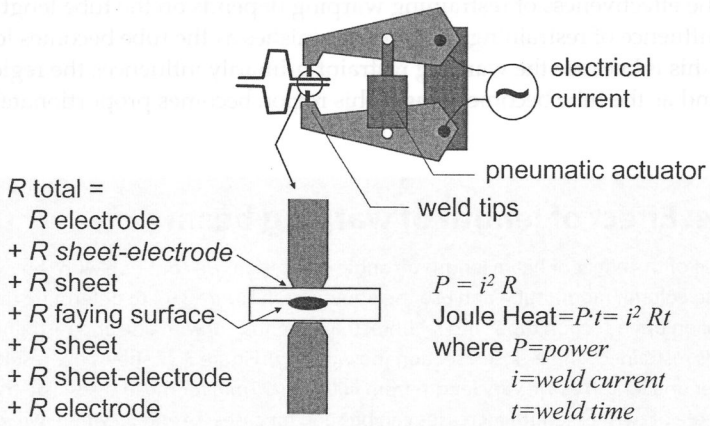

Figure 3.38 Spot welder.

3.3.4.1 Peel versus shear loading condition

Let us look at a single spot weld loaded by equal and opposite tensile loads, Figure 3.39. This condition is referred to as *shear loading*. The loads act on the centerline of the flange thickness, and the offset between centerlines creates a moment at the weld. The moment bends the flange and creates high stress in the area of the weld, as shown in Figure 3.40. Even the small offset of loads under shear loading creates stress concentrations, which reduce fatigue performance. Figure 3.41 shows this effect for a mild steel sample loaded in shear with the fatigue limit being reduced from the base material—in this case, by a factor of seven. When an adhesive is used in addition to the spot weld, the stresses are more evenly distributed and the fatigue performance is enhanced.

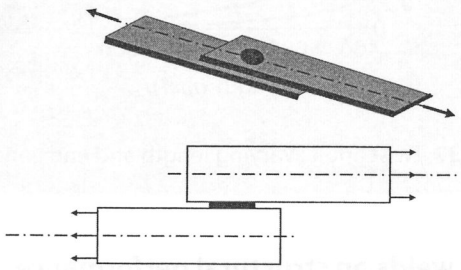

Figure 3.39 Shear-loaded spot-welded joint.

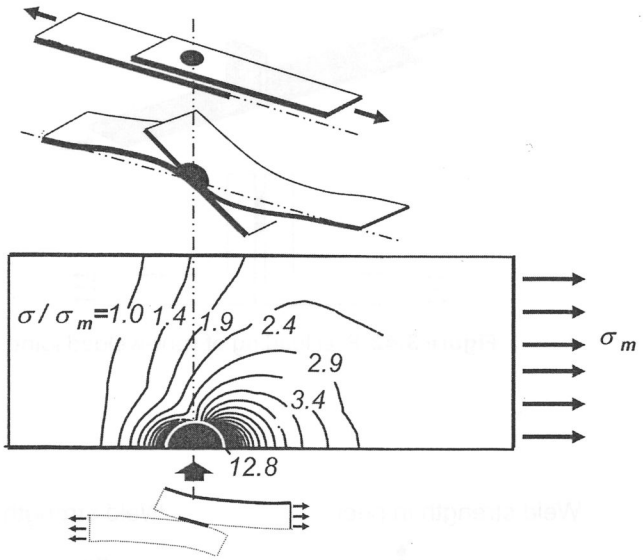

Figure 3.40 Stress in spot-welded joint.

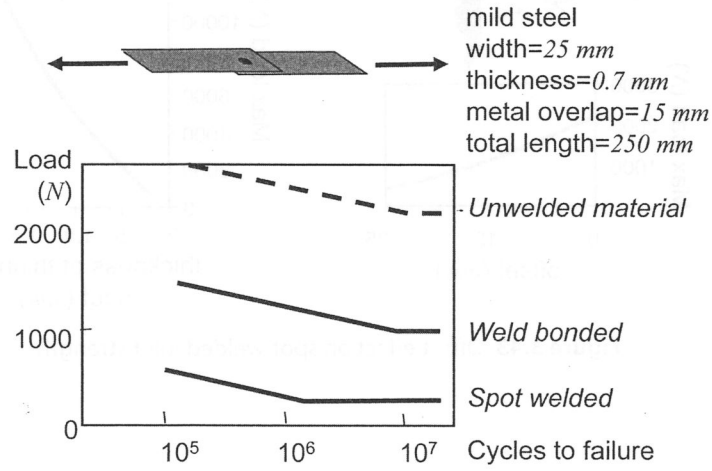

Figure 3.41 Fatigue of spot-welded joint in shear.

Another loading configuration—*peel loading*—increases this detrimental offset even more, Figure 3.42. Comparing weld strength for an individual weld, Figure 3.43, shows the effect of increasing the loading offset, x, beyond the sheet thickness as in shear loading. Because of this effect, good design practice is to use part geometry to put welds into *shear loading* rather than *peel loading*. Figure 3.44 and 3.45 show auto body examples for welds in peel and the preferred design with the weld in shear. Note that in each case, we assume a tensile load within the plane of the thin-wall material, and attempt to minimize the offset of this tensile load from the weld.

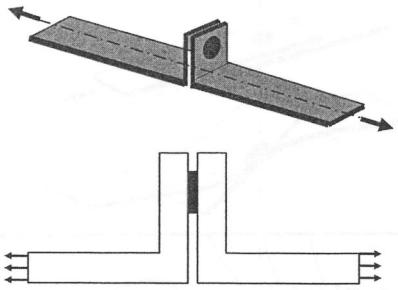

Figure 3.42 Peel loading of spot-welded joint.

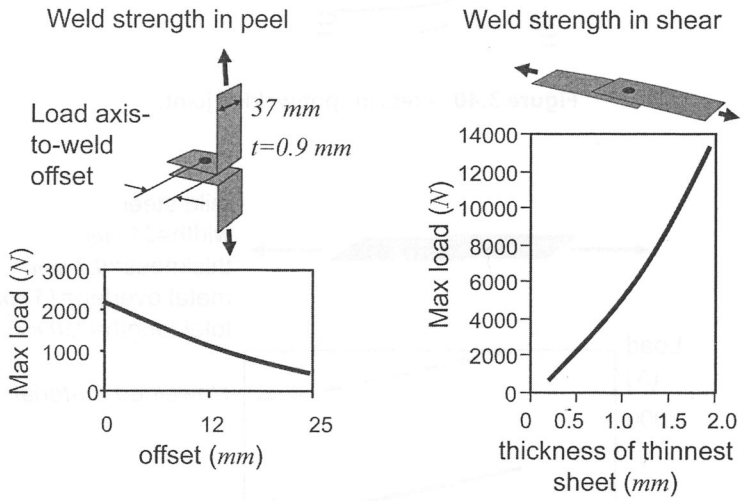

Figure 3.43 Offset effect on spot-welded joint strength.

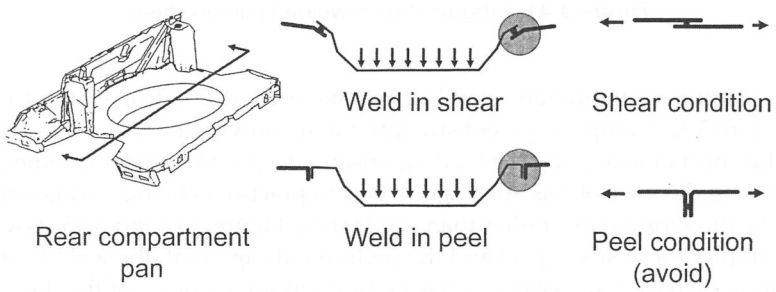

Figure 3.44 Examples of rear compartment joints in shear and peel.

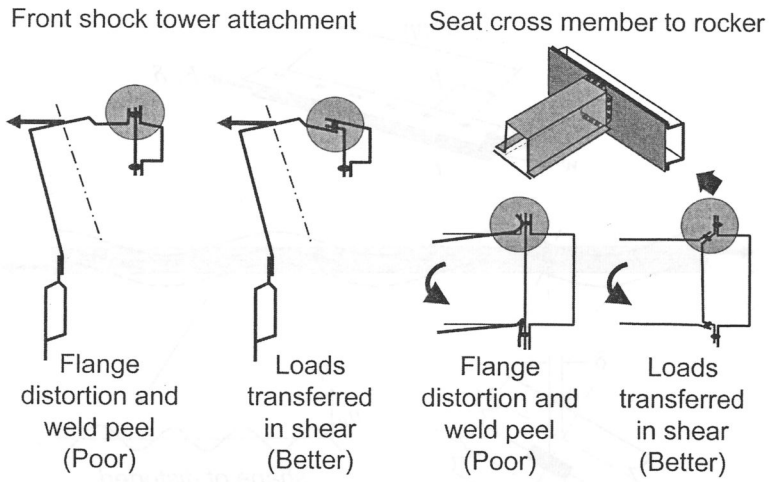

Figure 3.45 Examples of joints in shear and peel.

3.3.4.2 Longitudinal stiffness of a shear-loaded weld flange

Even with a well-designed spot-welded joint under shear loading, local deformations, which will reduce the apparent stiffness of a section, will occur. We will now look at a welded flange and determine how it elastically deforms under the action of shear loading. Isolating one spot weld, the distortion under a shear load is a rotation with the center at the interface of the weld, Figure 3.46. This rotation causes a relative longitudinal deflection between the two flanges. Now looking at a series of welds under shear loading, we can expect the deformation shown in Figure 3.47.

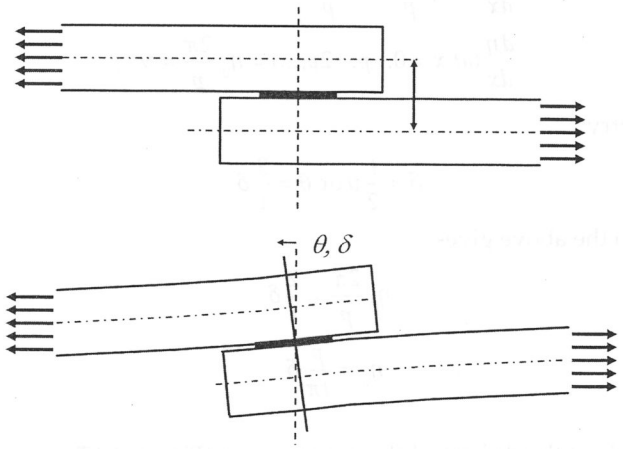

Figure 3.46 Distortion at spot weld.

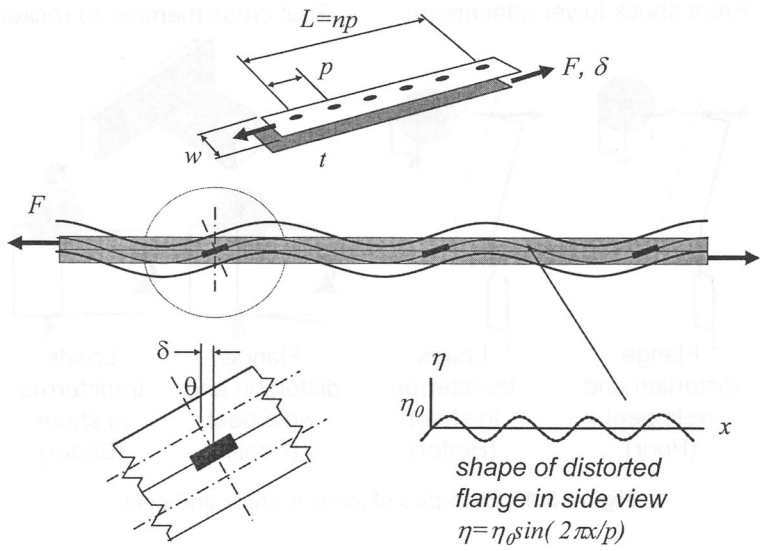

Figure 3.47 Distortion for a series of spot welds.

At each weld the same small rotation occurs and the result is a relative longitudinal deflection at the end of the flanges. Let the deflected shape of the flange be given as:

$$\eta = \eta_0 \sin\frac{2\pi x}{p}$$

At each weld, the slope is θ at $x=0, p, 2p \ldots$:

$$\frac{d\eta}{dx} = \eta_0 \frac{2\pi}{p}\cos\frac{2\pi x}{p}$$

$$\frac{d\eta}{dx}(at\ x = 0,\ \ p,\ \ 2p,\ldots) = \eta_0 \frac{2\pi}{p} = \theta$$

From the geometry:

$$\delta = \frac{t}{2}\theta \text{ or } \theta = \frac{2}{t}\delta$$

Substituting into the above gives:

$$\eta_0 \frac{2\pi}{p} = \frac{2}{t}\delta$$

$$\eta_0 = \frac{p}{t\pi}\delta$$

where:

η_0 = Amplitude of the deformed flange sine wave (Figure 3.47)

t = Thickness for upper and lower flange

p = Spot weld pitch (distance between spot welds)

δ = Lateral deflection of the flange from the original position

We can now use energy principles and equate work done by the external shearing force to the strain energy stored in bending the flange into the sinusoidal shape.

The work done by an external elastic shearing force acting through distance δ is:

$$work = \frac{1}{2}F\delta = \frac{1}{2}(qL)\delta = \frac{1}{2}(qnp)\delta$$

where:

q = Shear flow at the welded flange

n = Number of spot welds in the length

p = Weld pitch (distance between spot welds)

δ = Deflection down the length of the welded flange

The bending strain energy in the distorted flange with moment of inertia I is:

$$e = \int_0^L \frac{EI(\eta'')^2}{2}dx \quad \text{and} \quad \eta'' = -\eta_0\left(\frac{2\pi}{p}\right)^2 \sin\frac{2\pi x}{p}$$

$$e = \frac{EI}{2}\int_0^{L=np}\left[-\eta_0\left(\frac{2\pi}{p}\right)^2 \sin\frac{2\pi x}{p}\right]^2 dx$$

$$e = \frac{EI}{2}\eta_0{}^2\left(\frac{2\pi}{p}\right)^4 \int_0^{L=np} \sin^2\left(\frac{2\pi x}{p}\right)dx$$

Substituting the identity and integrating:

$$\sin^2\left(\frac{2\pi x}{p}\right) = \frac{1-\cos 2\left(\frac{2\pi x}{p}\right)}{2}$$

$$e = \frac{EI}{2}\eta_0{}^2\left(\frac{2\pi}{p}\right)^4 \frac{np}{2}$$

$$\text{from above } \eta_0 = \frac{p}{t\pi}\delta \text{ so}$$

$$e = \frac{4EI\pi^2}{t^2}\frac{n\delta^2}{p}$$

Now equating work with strain energy gives:

$$\frac{1}{2}(qnp)\delta = \frac{4EI\pi^2}{t^2}\frac{n\delta^2}{p}$$

$$q = \frac{8EI\pi^2}{(pt)^2}\delta$$

For a flange width, w, and thickness, t, $I=wt^3/12$ and:

$$\delta = \frac{3p^2}{2E\pi^2 wt}q \tag{3.16}$$

where:

δ = The deflection down the length of the welded flange

p = Weld pitch (distance between spot welds)

q = Shear flow across welded flanges (force per unit length)

E = Young's Modulus

w = Flange width

t = Flange thickness

Equation 3.16 provides some insight into the added flexibility when a spot-welded flange is present in a section. When a shear load is introduced at the weld interface, a longitudinal deflection will occur. This deflection is proportional to the square of the weld pitch. The deflection occurs whenever a shear across the weld is present, during both section bending or in torsion. To illustrate the influence on section stiffness, consider a tube, closed by a single spot-weld flange, Figure 3.48.

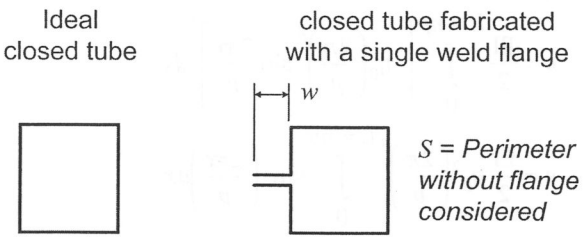

Figure 3.48 Closed tube with single weld flange.

The tube of Figure 3.48 is twisted by torque, T, and we are interested in the angle of deflection [7]. In our previous development of the closed-tube twisting behavior, we used a balance of work performed by the external torque to the internal shear strain energy within the tube. We can consider the same balance, but now the internal energy is also contained within the distorted weld flange.

External work = (shear strain energy in tube wall) + (strain energy in distorted flange)

$$\frac{1}{2}T\theta = \frac{SL}{2Gt}q^2 + \frac{1}{2}(qL)\delta$$

Using the result of Equation 3.16 for δ:

$$\frac{1}{2}T\theta = \frac{SL}{2Gt}q^2 + \frac{1}{2}(qL)\left(\frac{3p^2}{2E\pi^2 wt}q\right)$$

Which can be simplified using the relationship, $\frac{G}{E} = \frac{1}{2(1+\mu)}$ to:

$$\frac{T}{\theta} = \frac{(stiffness\ of\ closed\ tube\ without\ weld\ flange)}{\left[1 + \frac{3}{4\pi^2(1+\mu)}\frac{p^2}{wS}\right]} \tag{3.17}$$

where:

(T/θ) = Torsional stiffness of the spot-welded tube

p = Weld pitch

μ = Poisson's ratio

w = Flange width

S = Perimeter of the section without flange considered

This expression gives an estimate of the reduced stiffness in a twisted section when a single spot-welded flange is present.

Example: Spot-weld flange

Consider once again the slotted steering column mounting section, Figure 3.30. Let us close the section with a single spot-welded flange, Figure 3.49. From Equation 3.17, the factor

$$\psi = \frac{1}{1+\dfrac{3}{4\pi^2(1+\mu)}\dfrac{p^2}{wS}}$$

is the fraction of the closed tube stiffness which will remain when the section is closed by a spot welded flange. Choosing typical values for the flange; *w=8 mm, t=1 mm* and varying the weld pitch over the range *40 mm < p < 60 mm*, we see the tube stiffness with the weld is reduced to between *85%* to *96%* of the closed wall stiffness, Figure 3.50.

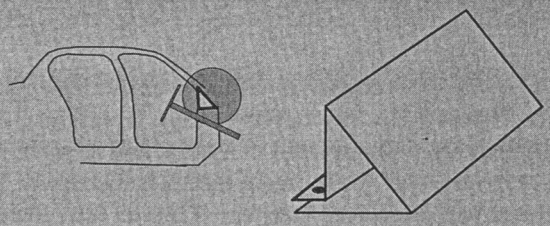

Figure 3.49 Steering column section with spot weld.

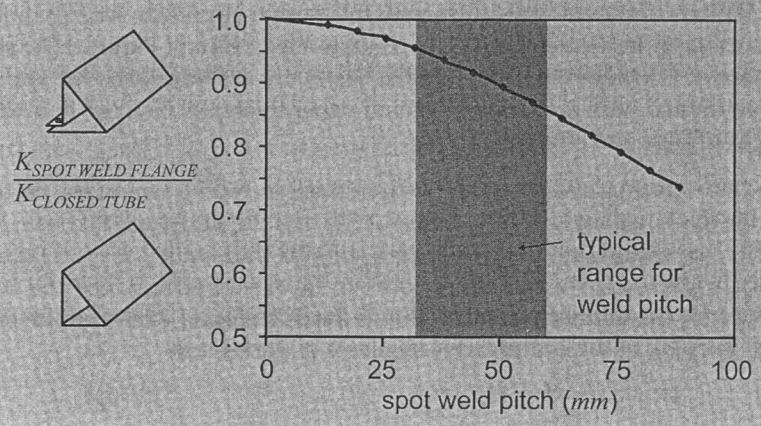

Figure 3.50 Spot weld spacing effect.

3.4 Thin-Wall Beam Section Design in Automobiles

In the previous sections, we have been discussing the unique behavior of the thin-wall sections used in the automotive body. It is helpful to ask a fundamental question: Why are automotive sections so often thin walled? We will use a simple thought experiment to answer this question. Consider a steel cantilever beam with a tip load. In this experiment the cross-section area is fixed (and therefore the beam mass is fixed), and we are free to choose the cross-section shape to maximize strength and stiffness. From basic beam theory we know for a cantilever beam that:

$$K = \frac{3EI}{L^3} \quad \text{and} \quad F_{MAX} = \frac{I\sigma_{DESIGN}}{Lc} \tag{3.18}$$

where:

K = Stiffness in bending

F_{MAX} = Maximum load (strength)

E = Young's Modulus

L = Beam length

c = Distance from the neutral axis to the outer fiber

I = Moment of inertia, $I=\int z^2 dA$

σ_{DESIGN} = Allowable design stress

In this experiment we will take the material yield stress as the design stress, $\sigma_{Design}=\sigma_Y$.

First let us imagine a square cross section of unit area as our base for stiffness and strength performance, Figure 3.51a. Now observe from Equations 3.18 that both stiffness and strength increase with moment of inertia, and as section material is moved away from the neutral axis the moment inertia is increased. This observation leads to an I beam shape with increased moment of inertia for constant cross-section area, yielding improved strength *and* stiffness. For example, Figure 3.51b shows an I beam of the same mass as the base square, resulting in 17 times the base stiffness. With no apparent difficulties with this design approach, we can move the material further from the neutral axis to result in the I beam of Figure 3.51c and a performance of 115 times the base stiffness. Given our assumptions, this approach could be continued until a *very* tall I beam of paper thickness resulted in presumably a *very* high stiffness and strength.

If we now move from a strictly thought experiment to testing two of the designed sections, the thick-walled I beam of Figure 3.51b and the thin-walled I beam of Figure 3.51c, we would find that while very stiff, the thin-walled section fails at an unexpectedly low load. The difference between expected performance and actual performance for the thinner-walled section is the existence of a new failure mode—*elastic plate buckling* of the compressive elements of the section.

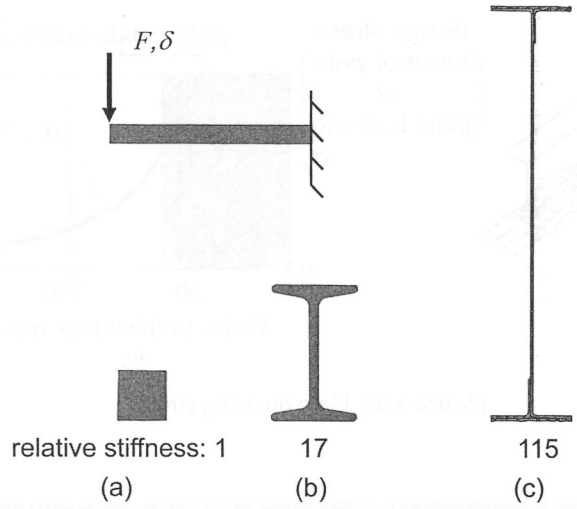

Figure 3.51 Relative bending stiffness for equal cross-section area.

The general behavior of a compressively loaded plate is to react loads by direct stress. However, if the plate is sufficiently thin, it bifurcates into the buckled shape, Figure 3.52. The compressive stress at which this occurs depends on the plate width-to-thickness ratio, *b/t*. The design stress for a thin plate under compressive loading is then the lower of yield stress or plate buckling stress, Figure 3.53.

Thus, in section design we deal with a trade-off: Thick-walled sections with higher strength but lower stiffness performance, or thin-walled sections with higher stiffness but lower strength performance due to plate buckling. Selection of the best section proportion then depends on the relationship of strength requirement to stiffness requirement for the section. This trade-off can best be illustrated with a specific automobile body design example.

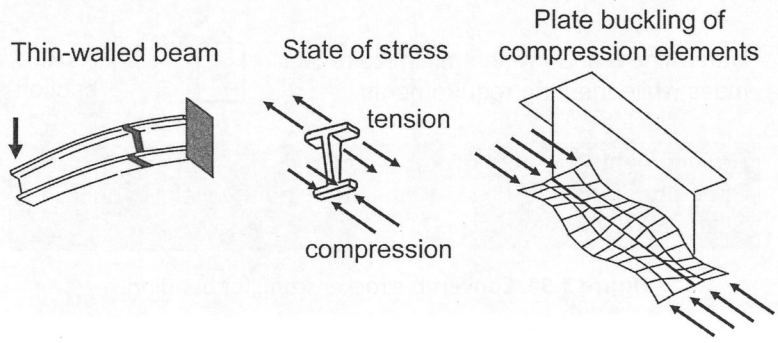

Figure 3.52 Deflection behavior of thin-walled members.

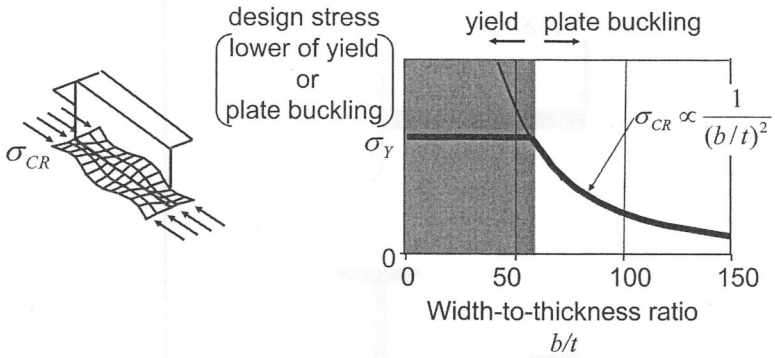

Figure 3.53 Plate buckling stress.

Example: Rocker sizing in convertible

Consider a highly idealized convertible, Figure 3.54 [8]. The bending performance of this vehicle is provided by the two rocker sections, which act as center-loaded simply supported beams. The specified bending stiffness requirement for this vehicle is *3335 N/mm* and strength requirement is *3335 N*. (The origin of global structure requirements will be discussed in subsequent chapters.) These requirements may be visualized graphically, Figure 3.55, with required performance shown as the shaded acceptable region. We wish to determine the mild steel rocker section width, *b*, and thickness, *t*, which meets both strength and stiffness requirements at a minimum mass. For this example we arbitrarily hold the section height at *1½* times the width.

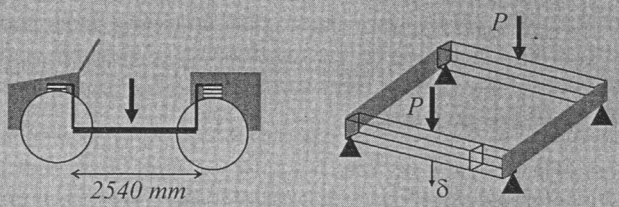

Determine *b* and *t* which minimize rocker mass while meeting requirements

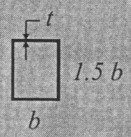

rocker section

Requirements for each rocker beam	
Strength-	*P>3335 N* failure either by yield or buckling
Stiffness *(P/δ)*	*K >3335 N/mm*

Figure 3.54 Convertible rocker sizing for bending.

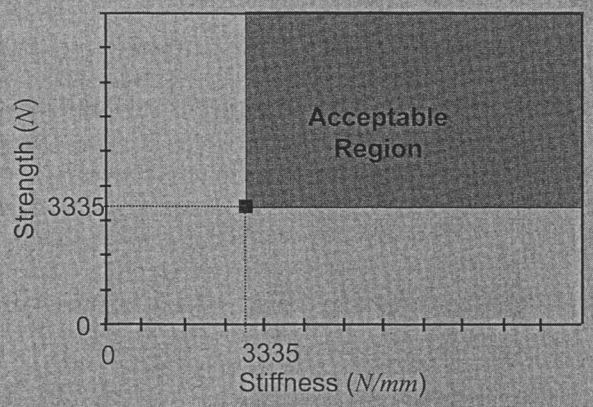

Figure 3.55 Convertible bending requirements.

Again using basic beam equations but now recognizing plate buckling as a possible failure mode, we have:

$$K = \frac{48EI}{L^3} \text{ and } F_{MAX} = \frac{4I\sigma_{DESIGN}}{Lc}, \tag{3.19 a, b}$$

$$\text{where } \sigma_{DESIGN} = Min\begin{pmatrix} \sigma_Y = 207N/mm \\ \sigma_{CR} = \dfrac{748355}{(b/t)^2} N/mm \end{pmatrix} \tag{3.19c}$$

(We will develop the above relationship for plate buckling stress later.) First, let us find when the failure mode will be yield and when it will be plate buckling of the compressive cap of the section. By equating yield stress to buckling stress in Equation 3.19c, the *(b/t)* ratio is found below which failure is by yield, and above which failure is by buckling:

$$\sigma_Y = \sigma_{CR}$$

$$207N/mm = \frac{748355}{(b/t)^2} N/mm$$

$$(b/t) \cong 60$$

We can now hold the cross-section area constant (constant mass rocker), and then vary *(b/t)* until a section meeting the requirements is found. Using section geometry, we can relate thickness and width to cross-section area, *A*, and width-to-thickness ratio, *(b/t)*:

$$t = \frac{b}{(b/t)} \quad \text{and} \quad b = \sqrt{\frac{A}{5}\left(\frac{b}{t}\right)} \tag{3.20}$$

Now we can choose a specific value for cross-section area and then vary width-to-thickness ratio. Using Equations 3.20 to calculate *b* and *t*, we can then calculate I and, using Equations 3.19 a & b, calculate the resulting body stiffness and strength. Let us first follow this procedure for sections which will fail by yield by using a width-to-thickness ratio range of $5<(b/t)<60$. Doing this for a cross-section area of $250\ mm^2$ gives the performance shown in Figure 3.56. Each data point represents a

section of cross-section area *250 mm²* (and mass *10.4 kg*) with the width-to-thickness ratios shown. As no section design for this cross-section area meets the requirements, we must choose a larger cross-section area. After some iteration, Figure 3.57 shows the result for a section with minimum area, *A=348 mm²* (and mass *14.5 kg*) and with *(b/t) = 60*, which satisfies the strength requirement, but not the stiffness requirement. We must continue to increase the area to *A=1232 mm²* (and mass *51 kg*) to meet both requirements with *(b/t)=60*. Notice that while just meeting the stiffness requirement, this section greatly exceeds the strength requirement. This is due to the constraints imposed by the Equations 3.19 with a design stress of yield.

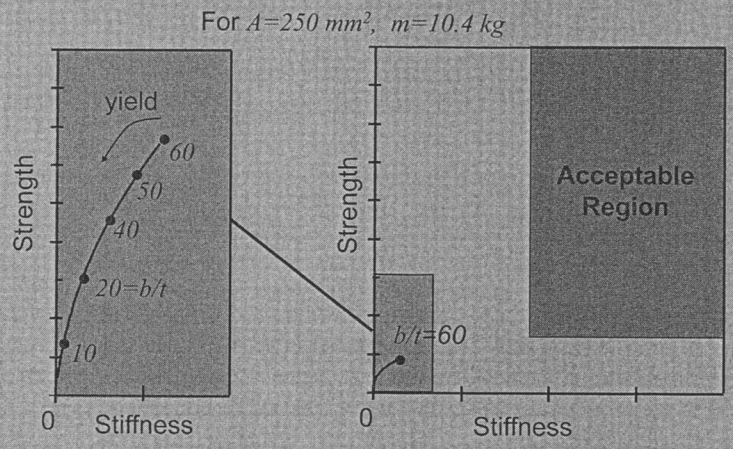

Figure 3.56 Thick-walled section performance.

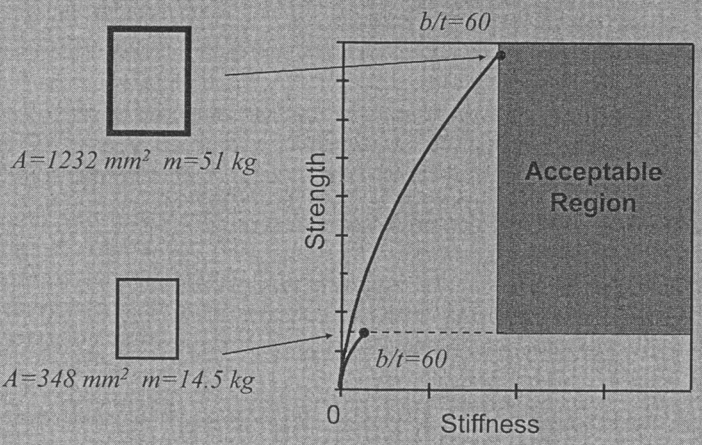

Figure 3.57 Thick-walled section performance meeting requirements.

Now let us allow the section to fail by plate buckling, and use a width-to-thickness ratio range of $60<(b/t)<160$. After some iteration, we find a section area of $A=832\ mm^2$ (and mass *34.5 kg*) and $(b/t)=135$, which meets both requirements simultaneously, Figure 3.58. Comparing the mass for these beams, Figure 3.59, we see that using the thin-wall section results in a considerable mass savings and a more efficient structure. Note that it is the specific relationship of strength requirement to stiffness requirement that leads to the optimal section proportion.

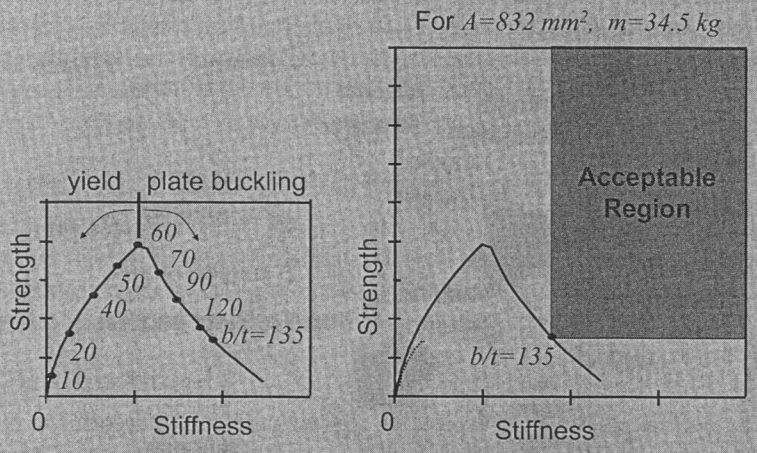

Figure 3.58 Thin-walled section performance.

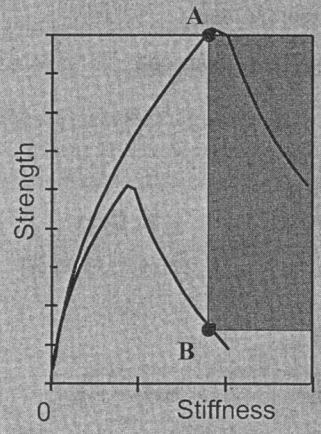

	b/t	failure mode	mass
A	60	yield	51.0 kg
B	135	plate buckling	34.5 kg

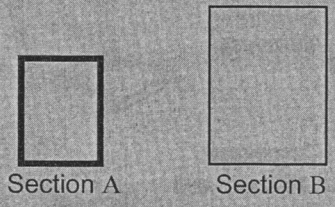

Figure 3.59 Mass savings of thin-walled section.

In the above example, we examined the motivation for using thin-walled sections for the case of global bending. Looking back at structural requirements for body subsystems, Figure 3.60, we can see that many of the subsystems, but not all, are stiffness dominated, and thin-wall sections are most efficient for those elements.

Understanding the relationship between section proportion and dominant requirement, we can look at an actual section and infer the dominant requirement for the section proportion. Figure 3.61 shows a typical automotive body structure with the measured

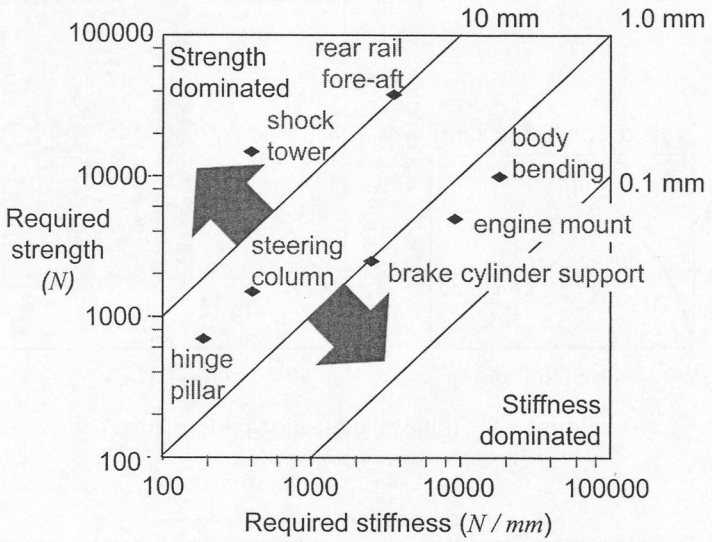

Figure 3.60 Dominant structural requirement.

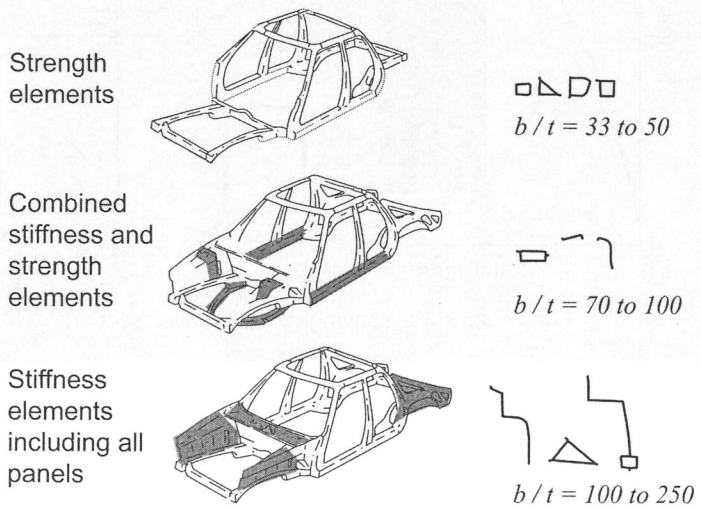

Figure 3.61 Section proportion determined by function

(b/t) ratios for various sections. For those sections with lower *(b/t)*, strength is the dominant requirement, and these sections are associated with reacting loads in a crash—roof crush, side impact, maintaining cabin integrity. For those sections with moderate *(b/t)*, a balance of strength and stiffness is required, and these sections are associated with major subsystem attachment points—suspension attachments and powertrain attachment. For those sections with high *(b/t)*, the stiffness requirement is clearly dominant, and these sections are associated with the overall stiffness of the body.

We have shown that many structural elements in automobile body design are dominated by stiffness requirements. A mass-effective means to design for stiffness performance is to use thin-walled sections which have a failure mode of buckling of the compressive section elements. In the next section, we will look at the governing equations for important modes of plate buckling.

3.5 Buckling of Thin-Walled Members

Perhaps the most significant difference between automotive sections and others is the failure modes caused by plate buckling of section elements. In this section we will develop tools to estimate plate buckling stress in section elements, and to estimate the strength of a buckled section.

3.5.1 Plate buckling

In the convertible rocker sizing example above, we used the expression:

$$\sigma_{CR} = \frac{748355}{(b/t)^2} N/mm$$

to describe the buckling stress for the compressive cap of the rocker section. We will now look at the physics of plate buckling and develop this and other buckling relationships.

Consider a flat plate of length a and width b where $a \geq b$, Figure 3.62. The plate lies in the x–y plane and is loaded by compressive stress, f_X, along the edges as shown. In the buckled state, the plate will have deflections, $w(x,y)$, normal to the plate in the z direction. For this analysis, we will consider the plate to have simply supported boundary conditions (no deflection and zero bending moment) along all edges.

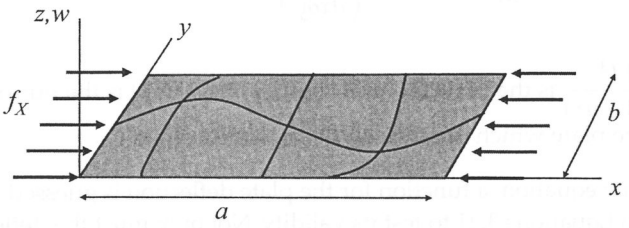

Figure 3.62 Flat plate.

Looking at a small element of this plate, we identify the loads acting, Figure 3.63. On the shaded y face of the element acts a bending moment per unit of length M_Y, which results in direct bending stresses σ_Y and a twisting moment, M_{XY}, which results in a

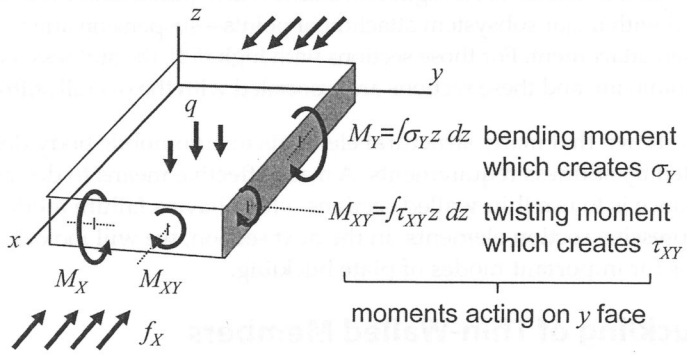

Figure 3.63 Plate element loading.

shear stress, τ_{XY}. Similar moments, M_X and M_{XY}, are applied to the x face. Also acting on the element is a normal load per unit of area, q, and a compressive stress, f_X.

By applying 1) static equilibrium of the element under these loads, 2) compatibility of deformations within the plate, and 3) the material stress-strain relationship, the plate equations result. For the development of these equations, the reader is referred to texts on the theory of elasticity [9, 10, 11].

$$\frac{\partial^4 w}{\partial x^4} + 2\frac{\partial^4 w}{\partial x^2 \partial y^2} + \frac{\partial^4 w}{\partial y^4} + \frac{f_X t}{D}\frac{\partial^2 w}{\partial x^2} + \frac{q}{D} = 0 \tag{3.21}$$

$$M_X = -D\left(\frac{\partial^2 w}{\partial x^2} + \mu\frac{\partial^2 w}{\partial y^2}\right)$$

$$M_Y = -D\left(\mu\frac{\partial^2 w}{\partial x^2} + \frac{\partial^2 w}{\partial y^2}\right)$$

$$M_{XY} = -D(1-\mu)\left(\frac{\partial^2 w}{\partial x \partial y}\right)$$

where $D = \dfrac{Et^3}{12(1-\mu^2)}$ is the plate flexural rigidity and $w(x,y)$ is the out-of-plane deflection of the plate which satisfies all these relationships.

To solve the plate equation, a function for the plate deflection is guessed and then substituted into Equations 3.21 to test its validity. Not only must the deflection satisfy the first of Equations 3.21, but the moments at the edges must satisfy the boundary conditions. For our case of a simply supported plate those boundary conditions are:

$$M_X(x=0,y)=0 \quad \text{and} \quad M_X(x=a,y)=0$$
$$M_Y(x,y=0)=0 \quad \text{and} \quad M_Y(x,y=b)=0$$

By observation of buckled plates, a reasonable guess at the deflected shape is:

$$w = A_{mn} \sin\left(\frac{m\pi x}{a}\right)\sin\left(\frac{n\pi y}{b}\right), \text{ where } m, n = 1, 2, 3, \ldots.$$

which satisfies the boundary conditions. (An example of this shape is shown in Figure 3.62 for *m=2, n=1.*) Substituting this assumed deformation into the first of Equations 3.21 with *q=0* gives:

$$\left[\pi^4\left(\frac{m^2}{a^2}+\frac{n^2}{b^2}\right)^2 - \frac{f_X t}{D}\frac{m^2\pi^2}{a^2}\right]A_{mn}\sin\left(\frac{m\pi x}{a}\right)\sin\left(\frac{n\pi y}{b}\right) = 0 \tag{3.22}$$

where *n, m = 1, 2, 3,. . .*

Since the term $A_{mn}\sin\left(\frac{m\pi x}{a}\right)\sin\left(\frac{n\pi y}{b}\right)$ is not in general zero, the term in brackets must be equal to zero, and solving for the compressive stress, f_X, yields:

$$f_X = \frac{D\pi^2}{tb^2}\left[m\left(\frac{b}{a}\right)+\frac{n^2}{m}\left(\frac{a}{b}\right)\right]^2 \tag{3.23}$$

where:

$f_X = \sigma_{CR}$, the critical plate buckling stress with all edges simply supported

D = Plate flexural rigidity $D = \dfrac{Et^3}{12(1-\mu^2)}$

t = Plate thickness

a = Plate length

b = Plate width (for the compressively loaded edge)

m = Number of half sine waves in buckled plate along x axis, *m=1, 2, 3 . . .*

n = Number of half sine waves in buckled plate along y axis, *n=1, 2, 3 . . .*

We would like to find the minimum compressive stress which would induce this deflected shape. This occurs at the minimum for the term in brackets. First observe that this term is, for all values of *m*, lowest when *n=1*. Physically, this occurs when the deflected shape across the plate is one half sine wave. To investigate the bracketed term with *n=1*, we plot it against plate length-to-width ratio, *a/b*, Figure 3.64. This plot shows for long plates where *a/b>1* a minimum value of four results. Thus the critical compressive plate buckling stress for a simply supported plate is then:

$$\sigma_{CR} = \frac{D\pi^2}{tb^2}4 = 4\frac{E\pi^2}{12(1-\mu^2)(b/t)^2} \tag{3.24}$$

Where variables are those of Equation 3.23. For plates where *a/b<1* use *m=1, n=1* in Equation 3.23 and:

$$\sigma_{CR} = \frac{D\pi^2}{tb^2}\left[\left(\frac{b}{a}\right)+\left(\frac{a}{b}\right)\right]^2 \tag{3.25}$$

Where variables are those of Equation 3.23. However, for most practical applications in automobile sections, *a/b>1* and Equation 3.24 is used when the boundary conditions are simply supported.

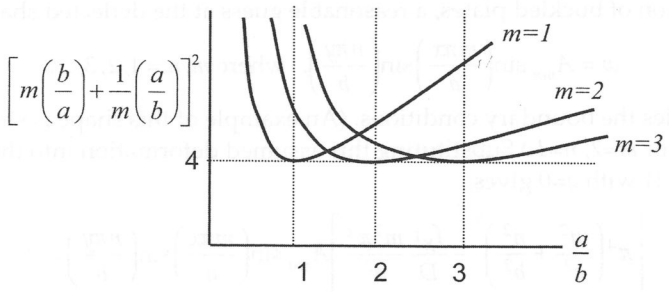

Figure 3.64 Buckling constant as function of (a/b).

Example: Plate buckling-1

To relate (*b/t*) ratio to critical stress, substituting values for mild steel *(E=207,000 N/mm², μ=0.3)* into Equation 3.24 yields:

$$\sigma_{CR} = 4\frac{(207000N/mm^2)\pi^2}{12(1-.3^2)(b/t)^2} = \frac{748355}{(b/t)^2} N/mm^2$$

which is the relationship used earlier in the convertible example.

The critical stress of Equation 3.24 was developed for simply supported boundary conditions. With different boundary conditions, the form of Equation 3.24 may still be used, but with a plate buckling coefficient, *k*, replacing the value of 4.

$$\sigma_{CR} = k\frac{E\pi^2}{12(1-\mu^2)(b/t)^2} \tag{3.26}$$

Figure 3.65 provides values for the plate buckling coefficient for several boundary conditions found in practice [11, 12, 13]. Note the inclusion of shear and bending

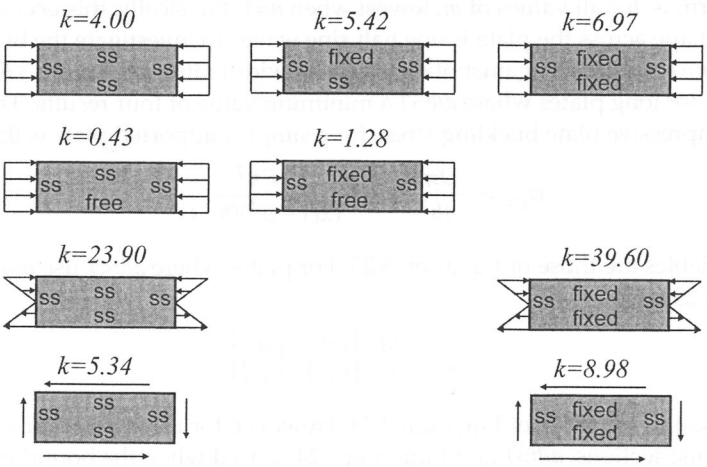

Figure 3.65 Buckling constant for long plates with various boundary conditions.

loading in this table. Whenever a plate is under a compressive state, it is subject to buckling. In the bending stress case, the plate is subject to buckling only in the compressive half of the web. In the shear case, Mohr's circle can be used to look at the stresses in an element rotated 45^o, Figure 3.66. It can be seen that, while the external loading is shear, on this rotated element one of the principle stresses is compression. Figure 3.67 shows the diagonal waves typical of a shear buckled plate.

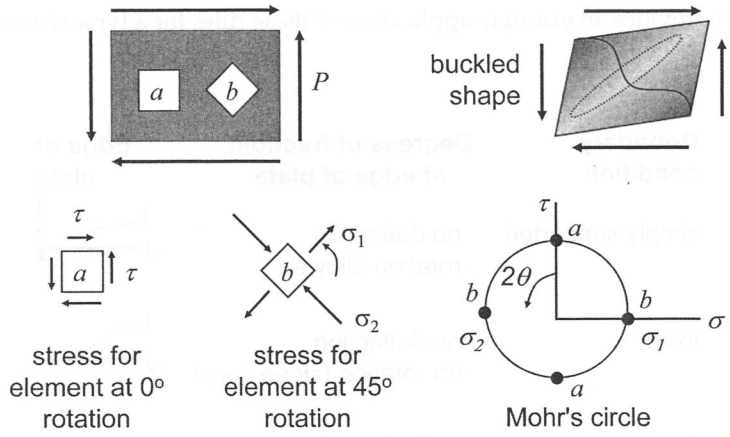

Figure 3.66 Compressive stress in a shear panel.

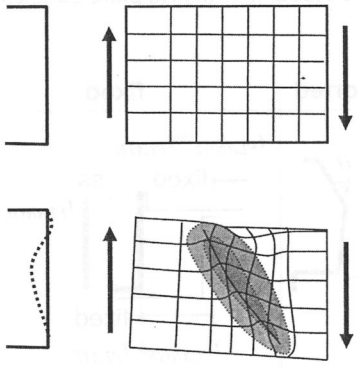

Figure 3.67 Shear buckled panel.

3.5.2 Identifying plate boundary conditions in practice

Our discussion of plate buckling has been in the context of automotive beam sections in which the plates are elements of the beam section. Given the complexity of automotive beam sections, it is at times difficult to choose the most appropriate boundary conditions and plate size. Our choices of simply supported, fixed, or free are highly idealized over the true physical constraint. Some general rules to help in this selection are shown in Figure 3.68a & b:

1. Each bent corner forms a simply supported boundary condition when the bent angle is greater than 40°. The plate width is then the distance from corner to corner.
2. When a plate is supported by a flange of thickness equal to or greater than the plate thickness, the boundary condition is fixed. The plate width is measured from the center line of the weld.
3. When an edge is unconnected, the boundary condition is free.

Figure 3.69 provides an example application of these rules for a typical automotive section.

Boundary condition	Degrees of freedom at edge of plate	Edge of plate
simply supported	·no deflection ·rotation allowed	
fixed	·no deflection ·no rotation (slope zero)	
free	·deflection allowed ·rotation allowed	

Figure 3.68a Identifying plate edge conditions.

simply supported	fixed	free
ss, ss, θ, for $\theta<40^o$, for $\theta>40^o$	$t_{FLANGE}=t_{PLATE}$ fixed, ss, $t_{FLANGE}<t_{PLATE}$, fixed, $t_{FLANGE}>t_{PLATE}$	free
Each bent corner with angle >40° is ss. For angle less <40°, plate extends to next corner	When a plate is supported by a flat flange where $t_{FLANGE}\geq t_{PLATE}$ the boundary condition is fixed. Otherwise boundary is ss.	Un-connected edge is free
plate size: corner to corner	plate size: from center line of weld	plate size: from edge

Figure 3.68b Identifying plate edge conditions.

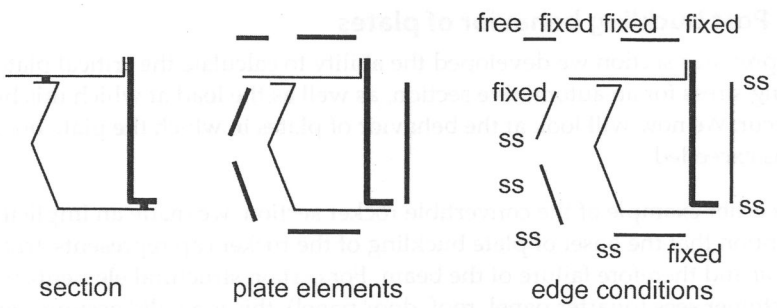

Figure 3.69 Example of plate edge conditions.

Example: Plate buckling-2

A *100-mm*-square thin-walled steel beam of thickness *0.86 mm* is loaded in compression. Determine the compressive load which will cause plate buckling in the section walls.

For this section, each of the four sides has a corner with a plate of the same thickness. The most appropriate boundary conditions are simply supported, with the plate uniformly loaded in compression. Using Figure 3.65, the buckling coefficient is $k=4$. The resulting critical stress using Equation 3.26 is

$$\sigma_{CR} = 4\frac{(207000N/mm^2)\pi^2}{12(1-.3^2)(100mm/0.86mm)^2}$$

$$\sigma_{CR} = 55.35N/mm^2$$

The load to cause this buckling on all four sides is

$$P_{CR} = \sigma_{CR}A = (55.35N/mm^2)\cdot 4(100mm\cdot 0.86mm)$$

$$P_{CR} = 19040N$$

Example: Plate buckling-3

A spot weld flange *(t=0.9 mm and b=15 mm)* is under uniform compressive stress down its length. See Figure 3.68b right side. Determine the stress at which the flange will buckle.

The flange has simply supported boundary conditions on three sides and is free on the fourth side. For this condition, the buckling coefficient is $k=0.43$ from Figure 3.65. Using Equation 3.26

$$\sigma_{CR} = 0.43\frac{(207000N/mm^2)\pi^2}{12(1-.3^2)(15mm/.9mm)^2}$$

$$\sigma_{CR} = 290N/mm^2$$

3.5.3 Post buckling behavior of plates

In the previous section we developed the ability to calculate the critical plate buckling stress for an automotive section, as well as the load at which this buckling will occur. We now will look at the behavior of plates in which the plate buckling stress is exceeded.

In the earlier example of the convertible rocker section, we made an implicit assumption that the onset of plate buckling of the rocker cap represents *excessive deflection* and therefore failure of the beam. For certain structural elements which the customer sees (quarter panel, roof, door panel), this is a valid assumption; a structural element with the out-of-plane buckling deformation would appear to have failed even though this deformation is elastic and will reverse when the load is removed. However, there are also non-visual structural elements for which the elastically buckled plate does not represent excessive deflection. For these elements the plate may be loaded beyond critical plate buckling before ultimate failure occurs. We now investigate the physical behavior of plates loaded beyond their critical stress, σ_{CR}.

To understand the post buckling behavior of a panel, first consider a slender beam with compressive loads at each end, Figure 3.70a. If the load is gradually increased, we will reach a critical load, $P_{CR}=\pi^2EI/L^2$, and the beam will undergo Euler buckling (not plate buckling). If we now attempt to increase the end load beyond the critical load, the beam will collapse. It has no ability to react increased load above the critical beam buckling load. Compare that behavior to that of a buckled plate, Figure 3.70b. Gradually increasing the compressive edge load, we will reach the plate buckling stress and the plate will bifurcate into the buckled pattern of deformation. However, unlike the slender beam, the load can continue to increase without collapse of the plate. Eventually an ultimate compressive load, Figure 3.70b, will be reached.

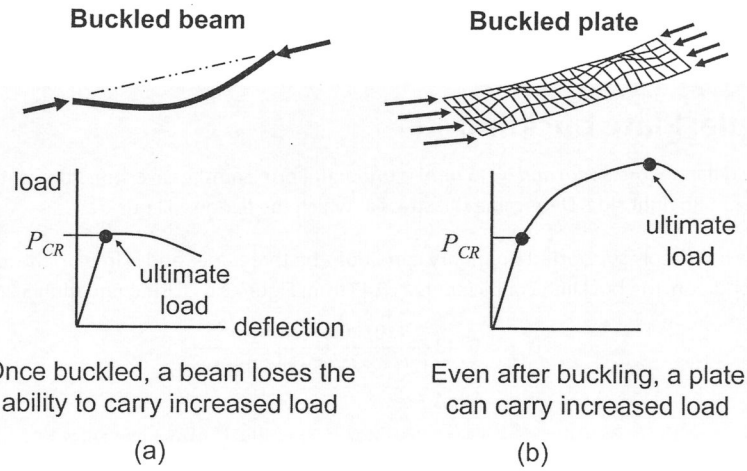

Figure 3.70 Comparison of buckling behavior.

For those cases where the mere visual detection of a buckled pattern does not represent excessive deformation, we would like to use this additional load-carrying capacity of the buckled plate. We begin by looking at a simply supported plate with an increasing compressive edge load, Figure 3.71a, and consider the stress across the plate at a section some distance from the applied load. Below the plate buckling stress, the stress distribution across the plate will be uniform and is given by $\sigma=P/(bt)$. As the load is increased to plate buckling, the stress remains uniform with $\sigma_{CR}=P/(bt)$, Figure 3.71a. Continuing to increase the load above critical plate buckling, the stress distribution across the plate becomes nonlinear. The stresses at the edges of the plate increase more rapidly than the stress at the center of the plate, Figure 3.71b. Eventually, by further increasing the load, the stress at the edges of the plate reaches the material yield stress and the plate exhibits an ultimate failure.

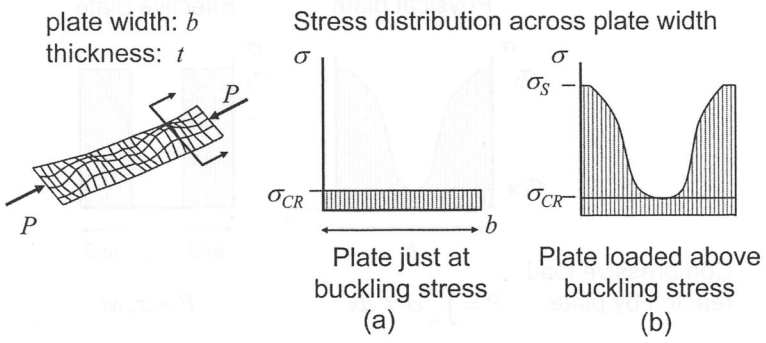

Figure 3.71 Post buckling stress distribution.

The difference between the load where a plate buckles and the load where the buckled plate yields can be considerable, and for efficient structures we must take advantage of this post buckled load carrying ability. In the next section, we will develop tools to do this.

3.5.4 Effective width

In many plate applications, we need to know the relationship between the applied compressive load, P, and maximum stress in the plate, σ_s, after elastic plate buckling has occurred. A convenient means to calculate the P-σ_s relationship is to replace the real plate with an imaginary plate having an *effective width, w*, which is less than the real plate width, Figure 3.72 [14]. The effective plate is assumed to have a uniform stress of σ_s across it, Figure 3.73b.

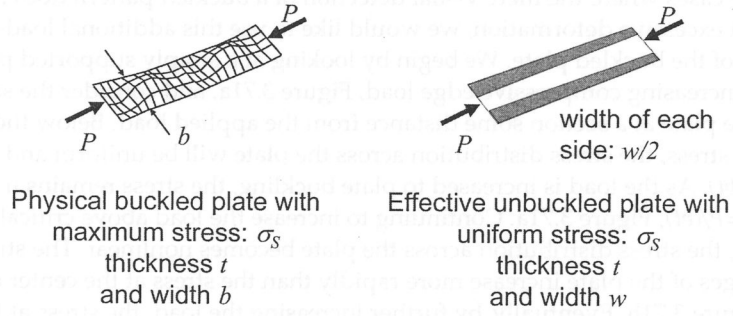

Figure 3.72 Effective width concept.

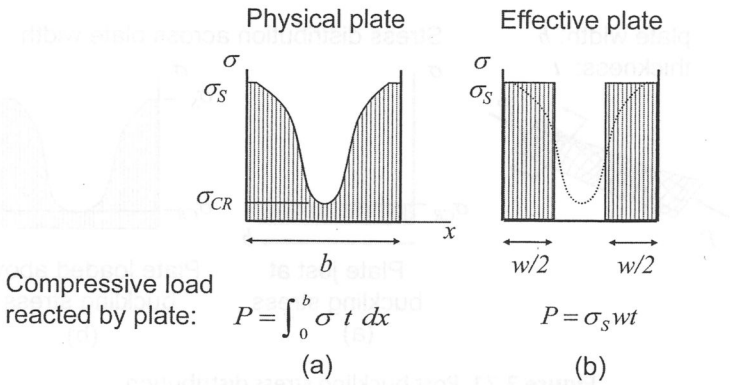

Figure 3.73 Determining effective width of a buckled plate.

For this effective plate, with currently unknown width w, the relationship between load and maximum stress is:

$$P_{\text{EFECTIVE PLATE}} = \sigma_S(wt) \tag{3.27}$$

where:

$P_{EFFECTIVE\ PLATE}$ = Load on plate

σ_S = Maximum stress on plate

w = Effective width of plate

t = Thickness of plate

We can use Equation 3.27 as a convenient way to calculate the applied load, P, given σ_S, providing we know the effective width, w. In the following, we develop a means to calculate the effective width given a maximum plate stress, σ_S.

Looking at the physical plate with non-uniform stress distribution and maximum stress, σ_S, Figure 3.73a, the applied compressive load is given by:

$$P_{\text{REAL PLATE}} = \int_0^b \sigma(tdx) \tag{3.28}$$

Looking at the general shape of the stress distribution for a buckled plate, Figure 3.73a, we take for the stress distribution across the plate:

$$\sigma = \left(\frac{\sigma_S + \sigma_{CR}}{2}\right) + \left(\frac{\sigma_S + \sigma_{CR}}{2}\right)\cos\frac{2\pi x}{b} \tag{3.29}$$

where $\sigma_S > \sigma_{CR}$

This function gives us a stress of σ_{CR} at the center of the plate and σ_S at the edges.

Now substituting Equation 3.29 into 3.28 and integrating yields:

$$P_{\text{REAL PLATE}} = tb\left(\frac{\sigma_S + \sigma_{CR}}{2}\right) \tag{3.30}$$

as the force applied to the buckled plate which results in a maximum stress σ_S.

Equating the load for each plate shown in Figure 3.73 and solving for the effective width, w, gives the desired result:

$$P_{\text{REAL PLATE}} = P_{\text{EFFECTIVE PLATE}}$$

$$tb\left(\frac{\sigma_S + \sigma_{CR}}{2}\right) = \sigma_S(wt)$$

$$w = \frac{1}{2}\left(1 + \frac{\sigma_{CR}}{\sigma_S}\right)b \tag{3.31}$$

where:

w = Effective width of plate under the stress σ_S

σ_{CR} = Buckling stress for plate

σ_S = Maximum stress on plate

b = Actual width of plate

The above relationship gives us the width of an imaginary effective plate which has a uniform stress of σ_S across it. When we are interested in the load to induce a maximum stress of $\sigma_S > \sigma_{CR}$ in a buckled plate, we can use Equation 3.31 to determine the effective plate and then Equation 3.27 to determine the load, P, to induce that maximum stress.

Example: Effective width-1

Consider that the earlier example of the *100-mm*--square thin-walled steel beam of thickness *0.86 mm* is loaded in compression. We determined the critical buckling stress for each side plate to be *55.35 N/mm²*, and the resulting compressive load to cause plate buckling to be *19040 N*. Now let us ask what load will cause a maximum stress of *111 N/mm²* in each plate.

In this example σ_S=*111 N/mm²* and σ_{CR}=*55.35 N/mm²*. Since $\sigma_S > \sigma_{CR}$ we are in the post buckling behavior for the plates, and we use Equation 3.31 to find the effective width of each of the four plates:

$$w = \frac{1}{2}\left(1 + \frac{55.35N/mm^2}{111N/mm^2}\right)100mm = 75mm$$

Now calculating the load on each plate using Equation 3.27

$$P_{EFFECTIVE\ PLATE} = 111N/mm^2(75mm \cdot 0.86mm)$$

$$P_{EFFECTIVE\ PLATE} = 7160N \text{ per side}$$

and for all four sides

P = 28640 N

Example: Effective width-2

A *100-mm*--square thin-walled steel beam of thickness *0.86 mm* is loaded by a bending moment, M_x, in the *x* direction using the right-hand rule. Under this moment, the maximum compressive stress in the top plate is *111 N/mm²*. What is the effective moment of inertia, $I_{EFFECTIVE}$, for the section under this moment loading?

In the previous example, we determined that *w=75 mm at* σ_S=*111 N/mm²*. The effective section is then shown in Figure 3.74. We replace the top plate with the effective plate; since the other three plates have not buckled, they are fully effective. We can now use standard tools to determine the moment of inertia for this effective section. We find that the centroid is *46.65 mm* up from bottom of section and $I_{EFFECTIVE}$=*5.16x10⁵ mm⁴* (90% of the nominal unbuckled section moment of inertia

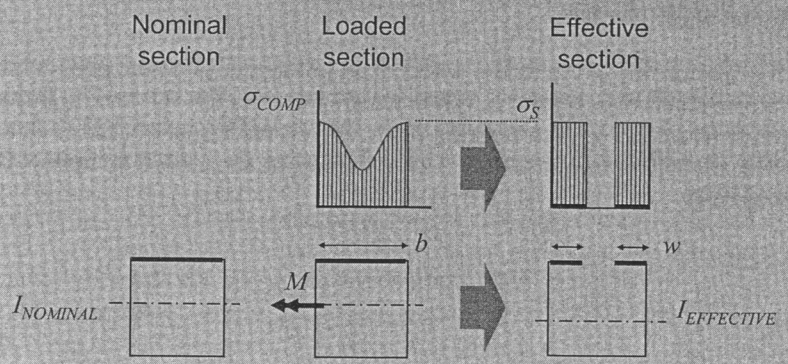

Figure 3.74 Reduced moment of inertia for beam with buckled element.

$I_{NOMINAL}=5.73x10^5\ mm^4$). This shows that once an element of a section has buckled, the moment of inertia is reduced and the effective stiffness of the beam is reduced since beam stiffness is proportional to *EI*.

Note, in this example we must also check the side walls of the section for buckling. This is done using Figure 3.65, selecting the case with simply supported boundary conditions and a linear stress distribution resulting in a buckling coefficient of $k=23.90$. Using Equation 3.26 we find that $\sigma_{CR}=331\ N/mm^2$ and we confirm that the side wall is not buckled.

Our selection for the true stress distribution across the buckled plate, Equation 3.29, is based on reasonable fit to the observed plate stress distribution and also computational convenience. Alternative empirical relationships for effective width shown below give more accurate results in practice. These relationships are compared in Figure 3.75:

$$w = 0.894b\sqrt{\frac{\sigma_{CR}}{\sigma_S}} \qquad (3.32a, b)$$

$$w = b\sqrt{\frac{\sigma_{CR}}{\sigma_S}}\left(1-0.22\sqrt{\frac{\sigma_{CR}}{\sigma_S}}\right)$$

where:

w = Effective width of plate under the stress σ_s

σ_{CR} = Buckling stress for plate

σ_S = Maximum stress on plate

b = Actual width of plate

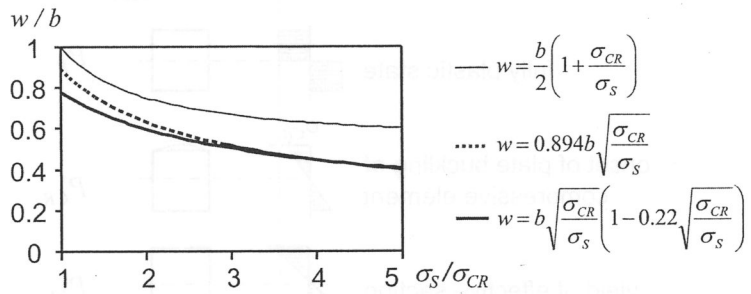

Figure 3.75 Comparison of effective width relationships.

3.5.5 Thin-walled section failure criteria

With the ability to calculate the compressive load acting on a buckled plate when given the maximum stress, we can now consider the ultimate failure load for the thin-walled plate. Extensive testing has been done on the ultimate load-carrying ability for a thin-wall section [15]. In these tests, a load was applied to a thin-walled square steel section as shown in Figure 3.76, and the peak load, P_{ULT}, was identified. Sections with a range of *(b/t)* ratio were tested from moderately thick walled, *(b/t)=50*, to highly thin walled, *(b/t)=200*. The measured ultimate load, P_{ULT}, was compared with five calculated values, Figure 3.77. These values include 1) the onset of yield at the outer fiber, P_Y; 2) fully plastic yield, P_P; 3) the onset of critical plate buckling, P_{CR}; 4) the onset of yield for the effective buckled section, P_{YE}; and 5) the onset of yield for a *U* section in which the compressive cap has been discarded, P_{YU}.

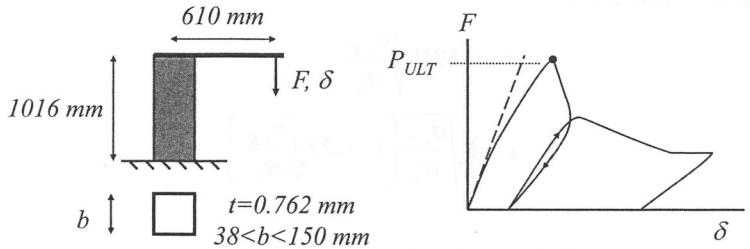

Figure 3.76 Behavior of square thin-walled sections. (Courtesy of SAE International)

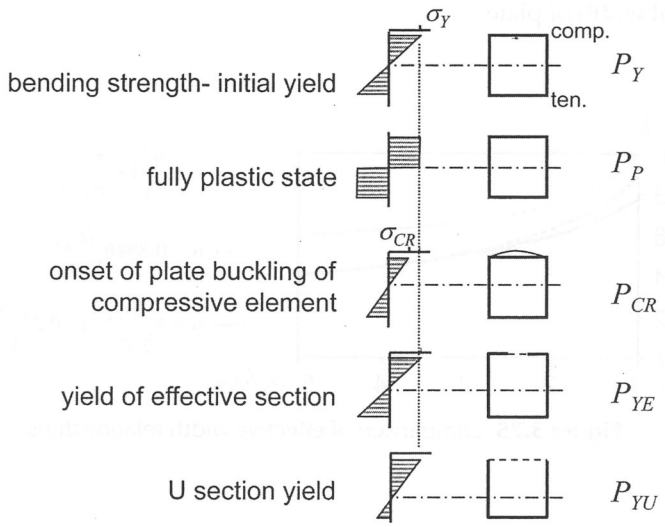

Figure 3.77 Physics of peak load – PULT. (Courtesy of SAE International)

The important result of this study is shown in Figure 3.78. For a wide range of *(b/t)* seen in automotive construction, the best predictor of ultimate load is P_{YE}, the onset of yield for the effective buckled section.

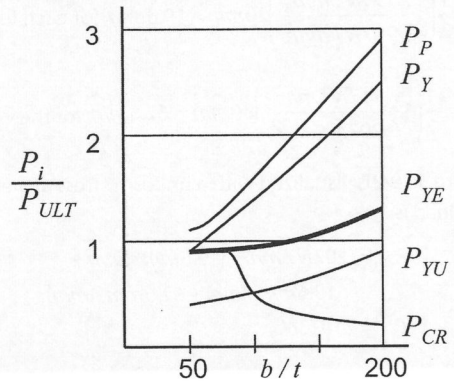

Figure 3.78 Ultimate load predicted by yield of effective section. (Courtesy of SAE International)

Example: Failure of a thin-walled beam

A Z section beam is part of a bumper reaction structure, Figure 3.79a. Calculate the ultimate compressive load for this section. The beam is stubby (i.e. will not Euler buckle as a beam), and the material is steel with σ_Y=*207 N/mm²*.

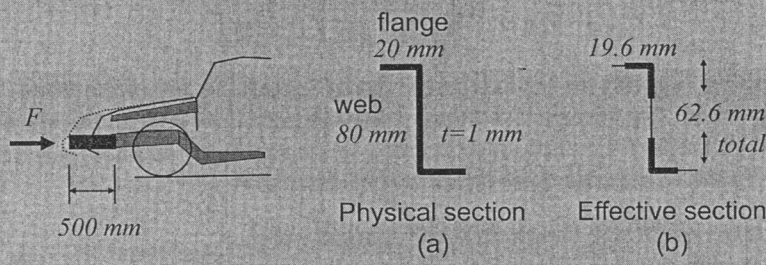

Figure 3.79 Bumper extension.

The ultimate load is given by P_{YE}, the onset of yield for the effective buckled section. First we find the plate buckling stress of each of the three plates which make up the Z section. Each of the two identical flanges have simply supported boundary conditions on three sides and are free on the fourth, so from Figure 3.65, *k=0.425*. Using Equation 3.26

$$\sigma_{CR} = 0.425 \frac{(207000 N/mm^2)\pi^2}{12(1-0.3^2)(20mm/1mm)^2} = 199 N/mm^2$$

for the flanges, and for the simply supported web *k=4*:

$$\sigma_{CR} = 4 \frac{(207000 N/mm^2)\pi^2}{12(1-0.3^2)(80mm/1mm)^2} = 117 N/mm^2$$

At a maximum stress equal to the material yield stress, $\sigma_s=\sigma_Y$, and from Equation 3.31, the effective width for each plate is:

$$w=\frac{1}{2}\left(1+\frac{199N/mm^2}{207N/mm^2}\right)20mm=19.6mm, \text{ for each flange}$$

$$w=\frac{1}{2}\left(1+\frac{117N/mm^2}{207N/mm^2}\right)80mm=62.6mm, \text{ for the web}$$

The effective section, Figure 3.79c, is visualized with a uniform stress at yield. Using Equation 3.27, the ultimate compressive load is:

$$P_{YE}=(207N/mm^2)(19.6mm\cdot 1mm+ 19.6mm\cdot 1mm+62.6mm\cdot 1mm)$$

$$P_{YE}=21073N$$

3.5.6 Techniques to inhibit buckling

From the above example, it can be seen that the existence of plate buckling reduces the ultimate load-bearing capacity of a section under compression. We may increase the strength of the section if somehow we can increase the critical plate buckling stress, σ_{CR}. In this section we look at ways to do this.

The plate buckling relationship, Equation 3.26, can be grouped as shown:

$$\sigma_{CR}=(k)\left(\frac{E\pi^2}{12(1-\mu^2)}\right)\left(\frac{1}{(b/t)^2}\right) \tag{3.33}$$

This grouping suggests means to increase σ_{CR} by increasing any of the three bracketed terms. The first enclosed term relates to boundary conditions, the second to normal stiffness of the plate, and the third to the width-to-thickness ratio. Several practical means to increase these terms will be discussed:

- Boundary conditions: flange curls and flanged holes
- Normal stiffness of the plate: material, curved elements, foam filling
- Width-to-thickness ratio: reducing width with beads and added edges.

The plate width may be reduced by adding beads to a section. By adding a longitudinal bead to a section, Figure 3.80, the plate width is effectively halved and the critical stress increased by a factor of four. Adding corners, Figure 3.81, can reduce plate width as shown, but in this case with some reduction in nominal moment of inertia as we are moving material closer to the neutral axis. Therefore, this technique is often used in sections under axial load as will be shown in the chapter on crashworthiness. Figure 3.82 is an example of adding corners to reduce plate width while maintaining moment of inertia.

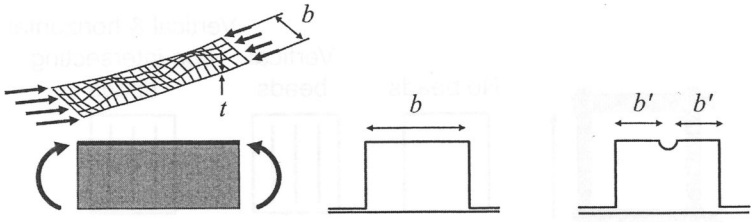

Figure 3.80 Reducing plate width by adding a bead.

Note: I is reduced but section is stiffer at increased loads due to buckling being inhibited

Figure 3.81 Reducing plate width by chamfering corners.

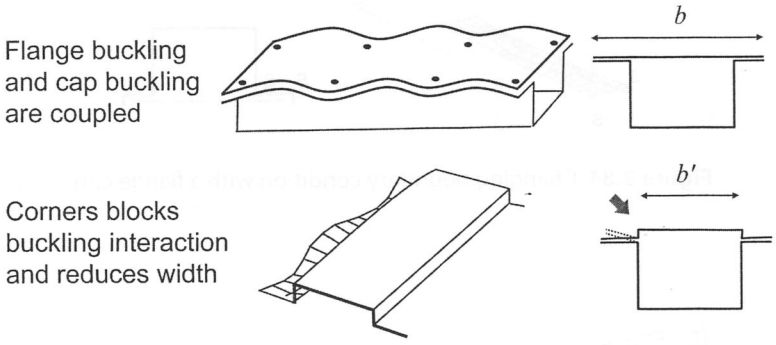

Figure 3.82 Reducing plate width by adding corners.

While we have focused on plates as elements of beam sections, the idea of increasing critical stress using added corners or beads also applies to panels where the loading is in shear, Figure 3.83. Note that for crossing bead patterns it is important that the beads do not fully intersect. Such intersections act as hinge points which reduce plate normal stiffness considerably.

An example of altered boundary condition is a flange with the addition of a flange curl, Figure 3.84. This changes the boundary conditions from free to simply supported with the buckling coefficient increasing from *0.425 to 4.0*. Similar increases in buckling stress are seen in panels with flanged holes, Figure 3.85.

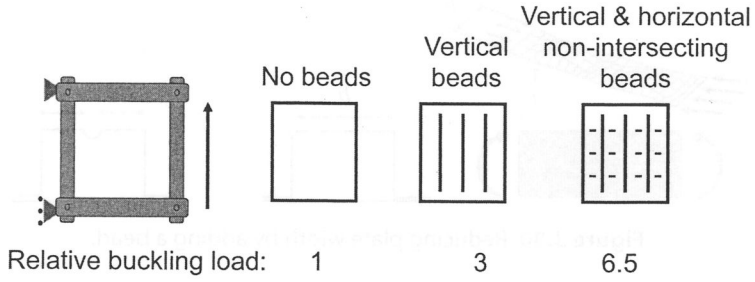

Figure 3.83 Reducing plate width using beads-shear case.

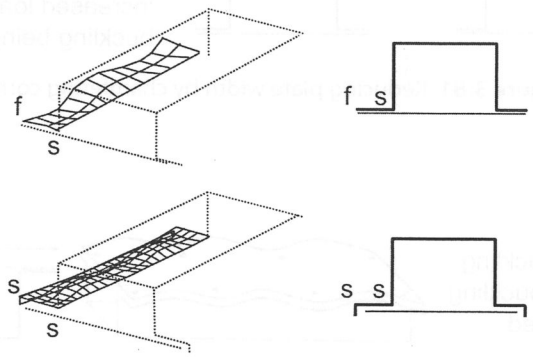

Figure 3.84 Changing boundary condition with a flange curl.

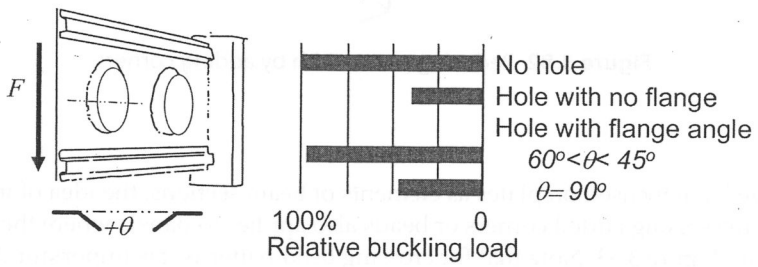

Figure 3.85 Flanged hole effect on shear buckling.

Plate normal stiffness can also be increased by curving the plate into a cylindrical element, Figure 3.86. This simple geometry change can increase critical stress dramatically [16, 17]. Yet another method to increase normal stiffness is by filling the beam section with foam. An example of the effects of foam filling is included in the section below on initial imperfections in plates.

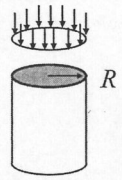

theoretical

$$\sigma_{CYL} = \frac{0.6\,tE}{R}$$

experiment

$$\sigma_{CYL} = \frac{0.25\,tE}{R}$$

Cylinder buckling

(a)

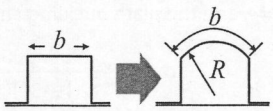

$$\sigma_{CR} = \frac{E}{6(1-\mu^2)}\left[\sqrt{\left(12(1-\mu^2)\frac{t^2}{R^2}+\frac{\pi^4 t^4}{b^4}\right)}+\frac{\pi^2 t^2}{b^2}\right]$$

$$\sigma_{SC} = \sqrt{\left(\sigma_{CYL}{}^2 + .25\sigma_{FLAT}{}^2\right)} + 0.5\sigma_{FLAT}$$

where $\sigma_{\_}$ is the buckling stress for:

σ_{SC} curved element

σ_{CYL} cylinder

σ_{FLAT} flat plate

Buckling of curved element

(b)

Figure 3.86 Buckling of curved elements.

Example: Inhibiting buckling

Consider again the Z section under compressive loading, but now with two buckling inhibiting techniques; a flange curl, and a central bead on the web, Figure 3.87. Again we are interested in the ultimate load.

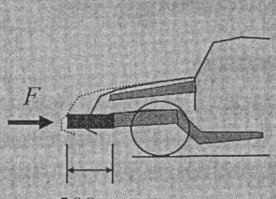

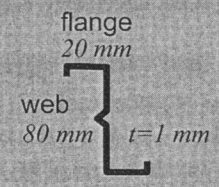

Physical section

(a)

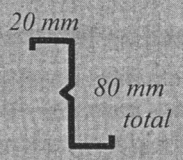

Effective section
(fully effective)

(b)

Figure 3.87 Bumper extension with section modifications.

With a flange curl, the boundary conditions for the flange are simply supported on all sides, with a resulting $k=4$. The plate buckling stress is for the stiffened flange:

$$\sigma_{CR} = 4\frac{(207000N/mm^2)\pi^2}{12(1-.3^2)(20mm/1mm)^2}$$

$$\sigma_{CR} = 1873N/mm^2$$

For the web with a central bead, we now have two plates of width $b=40\ mm$. With simply supported boundary conditions, $k=4$, and the plate buckling stress for the stiffened web:

$$\sigma_{CR} = 4\frac{(207000N/mm^2)\pi^2}{12(1-.3^2)(40mm/1mm)^2}$$

$$\sigma_{CR} = 468N/mm^2$$

Since both these critical stresses are above the material yield stress, the section is now fully effective and the ultimate load is:

$$P_{YE} = (207N/mm^2)(20mm \cdot 1mm + 20mm \cdot 1mm + 40mm \cdot 1mm + 40mm \cdot 1mm)$$

$$P_{YE} = 24840N$$

Compare to *21,073 N* for the unstiffened section.

3.5.7 Note on the use of high-strength steel

High-strength steels now make up a large portion of the steel used in automobile body structures. The motivation for this use is to gain higher strength and energy absorption at a reduced mass. Often this change in steel grade is done by direct substitution; only material and thickness is changed while keeping existing section geometry unchanged. It is important to recognize that because of plate buckling, the change in the strength is not directly proportional to yield stress. Take the previous Z section example with dual-phase steel, $\sigma_Y = 650\ N/mm^2$ *(94,000 psi)* substituted for mild steel, $\sigma_Y = 207\ N/mm^2$ *(30,000 psi)*. This substitution does not achieve a *(650/207)=3.14* times increase in strength because the buckling stress of the web, $\sigma_{CR} = 468\ N/mm^2$ *(68,000 psi)* is now below yield and the section is no longer fully effective as it was with mild steel. When substituting with higher-strength materials, it is important to reexamine the effective properties of a section and add buckling inhibitors which may not have been necessary with lower-strength steel.

3.5.8 Note on bifurcation and initial imperfection

The mathematical development of plate buckling considers an ideally flat plate which snaps instantly—bifurcates—from a flat plate to the buckled deformation. In practice, the plates making up the elements of an automotive section are imperfect, containing as-fabricated out-of-plane geometry.

To see the effect of this imperfection on buckling behavior, consider an edge view of a plate, Figure 3.88. Here we will greatly simplify our model to understand the most basic physics, and will consider an analogy to the plate—a beam supported by an elastic foundation of stiffness k_F *(N/mm/mm)*, Figure 3.89. The foundation stiffness represents, for example, the additional rigidity of foam filling the section.

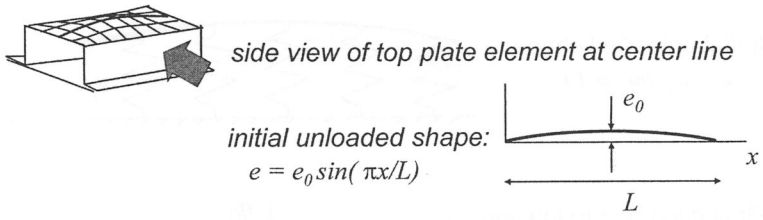

Figure 3.88 Initial imperfection in plate.

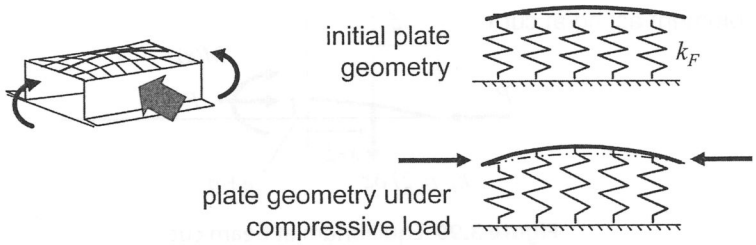

Figure 3.89 Elastic foundation model of initial imperfection.

The beam is given an initial unloaded 'imperfect' shape characterized by a half sine wave with amplitude e_0, Figure 3.90 top.

$$e = e_0 \sin(\pi x/L) \tag{3.34a}$$

The foundation springs in this initial condition are unstressed. The beam may deflect from this shape a distance $\eta(x)$ under the action of compressive end loads, P. We take as the deflected shape a half sine wave with amplitude η_0, Figure 3.90 center,

$$\eta = \eta_0 \sin(\pi x/L) \tag{3.34b}$$

Cutting the beam at a distance x from the end, Figure 3.90 bottom, the bending moment at the cut is

$$M(x) = -P(\eta + e) - \int_0^x k_F \eta(\xi)(x - \xi) d\xi \tag{3.34c}$$

substituting the expressions for e, Equation 3.34a, and η, Equation 3.34b, and integrating gives:

$$M(x) = \left[-P(\eta_0 + e_0) + k_F \eta_0 \left(\frac{L}{\pi} \right)^2 \right] \sin \frac{\pi x}{L}$$

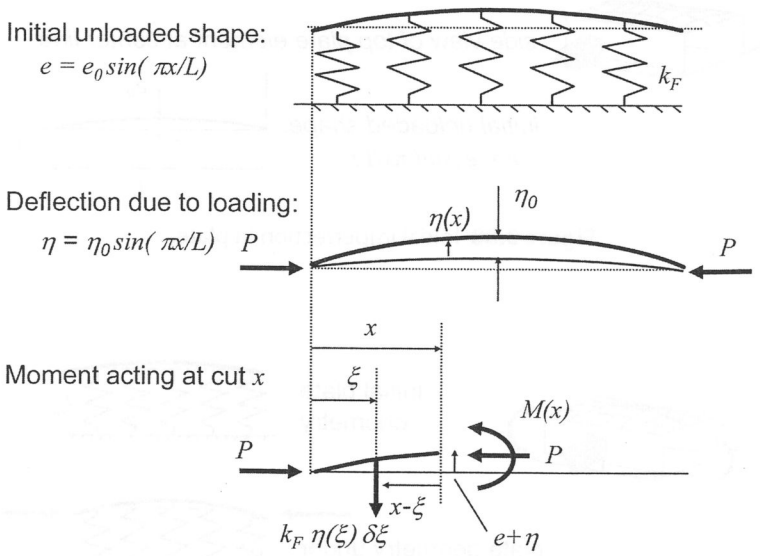

Figure 3.90 Equilibrium at beam cut.

Substituting Equations 3.34b and *c* into the beam equation:

$$\frac{\partial^2 \eta}{\partial x^2} = \frac{M}{EI}$$

gives the following result:

$$\frac{\eta_0}{e_0} = \frac{1}{\frac{P_{CR}}{P}\left(1+\frac{k_F}{EI}\right)-1} \tag{3.34d}$$

where:

P = Applied compressive load

P_{CR} = Euler buckling load, $P_{CR}=EI(\pi/L)^2$

e_0 = Initial out-of-plane imperfection

η_0 = Out-of-plane deflection

EI = Bending stiffness of plate

k_F = Stiffness per unit length which resists the out-of-plane deflection

Equation 3.34d gives us the deflection at the center of the beam, η_0, normalized to the initial imperfection magnitude, e_0. The deflection depends on the applied load, P, normalized to the critical Euler buckling load, P_{CR}.

First consider the behavior without any foundation stiffness, $k_F=0$. Equation 3.34d with $k_F=0$ yields

$$\frac{\eta_0}{e_0} = \frac{1}{\frac{P_{CR}}{P} - 1}$$

$$\frac{P}{P_{CR}} = \frac{\frac{\eta_0}{e_0}}{\frac{\eta_0}{e_0} + 1} \tag{3.34e}$$

Figure 3.91 plots the applied normalized compressive load, P/P_{CR}, against the lateral normalized deformation, η_0/e_0, at the center of the beam, Equation 3.34e. It can be seen that the existence of an initial imperfection tends to 'ease' the beam into the buckled shape rather than a sharp snap-over into the deflected shape at P_{CR}. While this model describes an imperfect *beam*, the physical behavior is analogous to a real plate with an initial imperfection.

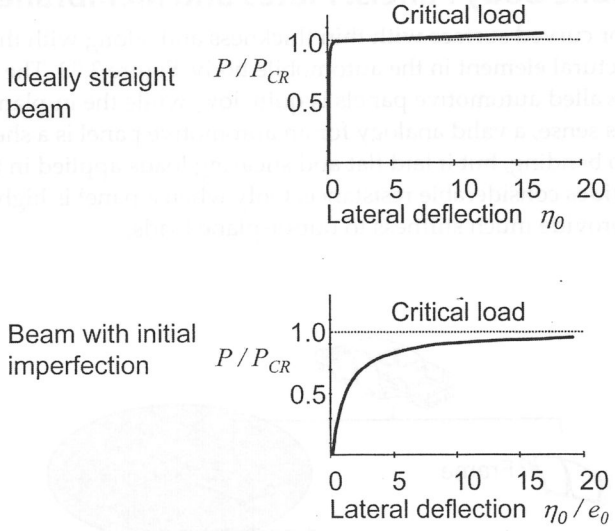

Figure 3.91 Buckling behavior with imperfection.

In the earlier section on inhibiting buckling, the technique of increasing the normal stiffness of the plate was mentioned. One embodiment of this technique is to foam fill a section. To buckle, a plate element of the section must also deflect the foam, and this action inhibits the onset of buckling by effectively increasing the normal stiffness of the plate. This can be modeled, Figure 3.89, as a beam (the plate) on an elastic foundation (the foam) by using Equation 3.34d. In this case, the factor $k_F/(EI)$ is the ratio of foam compressive stiffness to beam stiffness. Figure 3.92 shows the results of applying Equation 3.34d, and illustrates how the foam stiffness tends to increase the buckling load above the critical load for the unstiffened beam.

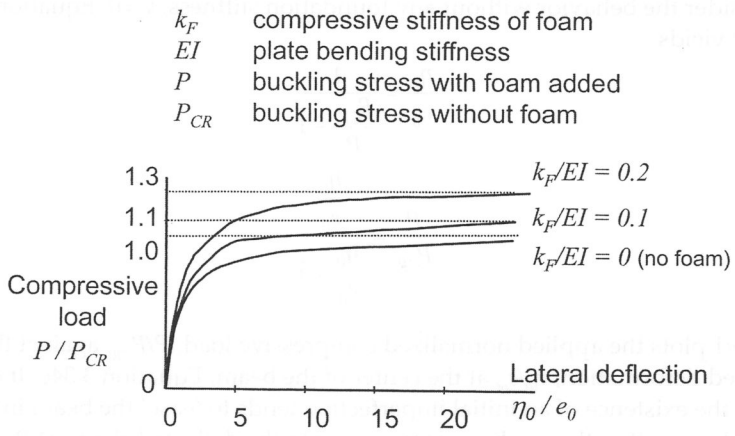

Figure 3.92 Plate buckling of a foam-filled section.

3.6 Automobile Body Panels: Plates and Membranes

A panel is a flat or curved surface with thin thickness and, along with the beam, is a primary structural element in the automobile body, Figure 3.93. The bending stiffness of thin-walled automotive panels is quite low, while the in-plane stiffness is quite high. In this sense, a valid analogy for an automotive panel is a sheet of paper: little resistance to bending, but if laid flat and shearing loads applied in the plane of the paper, it provides considerable resistance. Only when a panel is highly curved does it begin to provide much stiffness to out-of-plane loads.

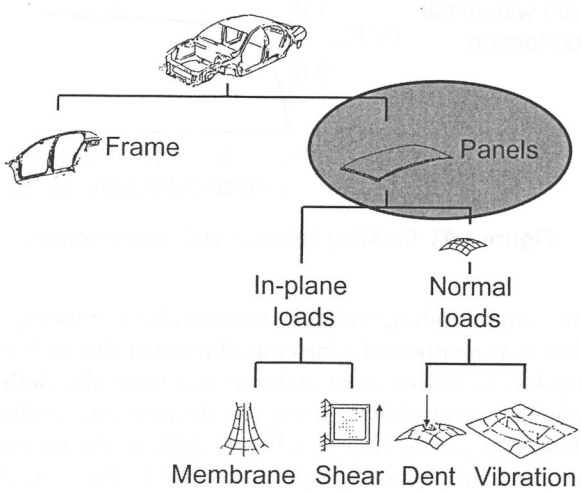

Figure 3.93 Loading classification for panels.

We will therefore divide the treatment of panels by the type of loads acting on the panel: normal loading of curved panels, and in-plane loading of flat or curved panels, Figure 3.93. In the next section we will look at loading of curved panels by a *point* load normal to the surface. Panels may also be loaded by a *distributed* normal load, for example by inertia during panel vibration; this topic will be treated later in the chapter on vibration.

3.6.1 Curved panel with normal loading

The exterior panels of an automobile are largely influenced by the overall styling of the vehicle. Because of this, structural performance is not the shape-defining function. However, a small set of structural requirements are used to screen valid shapes for curved exterior panels. These involve the reaction to normal point loading, which we will now discuss.

A curved panel loaded normal to the surface at a point exhibits complex load-deflection behavior, Figure 3.94. Initially, the load-deformation relationship is linear and elastic and can be characterized by a stiffness, K. At some higher load, the panel may begin to invert its curvature, Figure 3.94. This inversion may be either *soft*, where the surface stays in contact with the load applicator, or *hard*, where the surface snaps over and looses contact with the load applicator. The load where a hard snap-over occurs is referred to as the critical oil-canning load, P_{CR} (from the behavior of the bottom of an oiling can). A customer may judge the solidness of a panel by pushing with a thumb, and both K and P_{CR} relate to the customer perception of panel quality, with higher values being preferred.

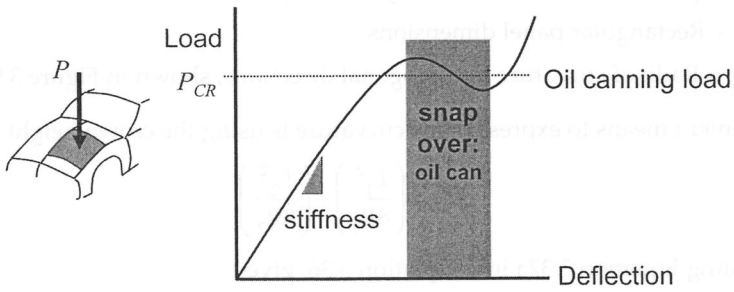

Figure 3.94 Curved panel behavior under normal load.

Dent resistance, another case of normal loading of panels, is measured by the kinetic energy of a dart, directed normal to a surface, which leaves a permanent dent in the panel. Again referring to Figure 3.94, this energy is proportional to the area under the load-deflection curve up to the point where permanent deformation occurs.

The properties of panel stiffness, oil-can load, and dent resistance for a curved panel are difficult to predict, and the equations below are a combination of analytical and empirical considerations. All equations assume simply supported boundary conditions for the panel [18, 19].

3.6.2 Normal stiffness of panels

In modeling the normal stiffness of automotive panels, we assume the panel is large and the distortion under a point normal load is localized and does not extend to the boundaries. First consider the theoretical normal stiffness of a partial spherical shell under a concentrated load:

$$K = \frac{B}{R}\frac{Et^2}{\sqrt{1-\mu^2}} \tag{3.35}$$

where:

R = Spherical radius ($R>>t$)

B = Constant: B=2.309 for a shallow shell, [6]

E = Young's Modulus

μ = Poisson's ratio

t = Panel thickness

Automotive panels are generally doubly curved—curvature not the same in two orthogonal directions—and Equation 3.35 can be generalized by replacing the spherical curvature ($1/R$) with:

$$\frac{1}{R_{EQ}} = \frac{\left(\frac{L_1^2}{R_1}\right)+\left(\frac{L_2^2}{R_2}\right)}{2L_1L_2} = \frac{1}{2}\left[\frac{1}{R_1}\left(\frac{L_1}{L_2}\right)+\frac{1}{R_2}\left(\frac{L_2}{L_1}\right)\right] \tag{3.36}$$

where:

R_{EQ} = Equivalent radius for a doubly curved panel

L_1, L_2 = Rectangular panel dimensions

R_1, R_2 = Radii of curvature in orthogonal directions, shown in Figure 3.96

A convenient means to express panel curvature is using the crown height H_C, where:

$$H_C = \left(\frac{L_1^2}{8R_1}\right)+\left(\frac{L_2^2}{8R_2}\right) \tag{3.37a}$$

Substituting Equation 3.37a into Equation 3.36, gives:

$$\frac{1}{R_{EQ}} = \frac{4H_C}{L_1L_2} \tag{3.37b}$$

To calculate normal stiffness for a doubly curved panel, use Equation 3.36 or 3.37 to determine the equivalent spherical radius, R_{EQ}, then substitute into Equation 3.35. The constant, B, in Equation 3.35 ranges from the shallow spherical value, B=*2.309* to B=*2.96* for a shallow doubly curved panel (H_C/t=*4*) to B=*3.618* for a deeper doubly curved panel ($20<H_C/t<60$) [18].

3.6.3 Oil-canning resistance

The critical buckling load, P_{CR}, at which the panel will bifurcate and reverse its curvature is given by

$$P_{CR} = \frac{CR_{CR}\pi^2 Et^4}{L_1 L_2 (1-\mu^2)} \tag{3.38}$$

where:

$C = 0.645 - 7.75x\ 10^{-7} L_1 L_2$ for $L_{1,2}$ in millimeters

$R_{CR} = 45.929 - 34.1832 + 6.397\lambda^2$

$$\lambda = .5\sqrt{\frac{L_1 L_2}{t}}\sqrt{\frac{12(1-\mu^2)}{R_1 R_2}}$$

valid over the range $\begin{cases} \frac{R_1}{L_1} \text{ and } \frac{R_2}{L_2} > 2 \\ \frac{1}{3} < \frac{L_1}{L_2} < 3 \\ L_1 L_2 < 0.774 m^2 \end{cases}$

3.6.4 Dent resistance

The denting resistance, W, is the minimum energy to dent the surface. Here the definition of a dent is a *0.025 mm (0.001 in)* permanent deformation in the panel. Dent resistance depends on σ_{YD}, the yield at a *dynamic* strain rate (rather than the more typical *static* value). The dynamic strain rate corresponding to denting (*10* to *100 /sec*) is many orders of magnitude higher than the typical static tensile test strain rate (*0.001 /sec*). The ratio of dynamic to static yield strength of steels at strain rates of up to *100 /sec* is shown in Figure 3.95. The denting energy, based on empirical curve fit, is [18]:

$$W = 56.8\frac{(\sigma_{YD} t^2)^2}{K} \tag{3.39}$$

where:

K = Panel normal stiffness (Equation 3.35)

t = Panel thickness

σ_{YD} = Yield strength at a dynamic strain rate

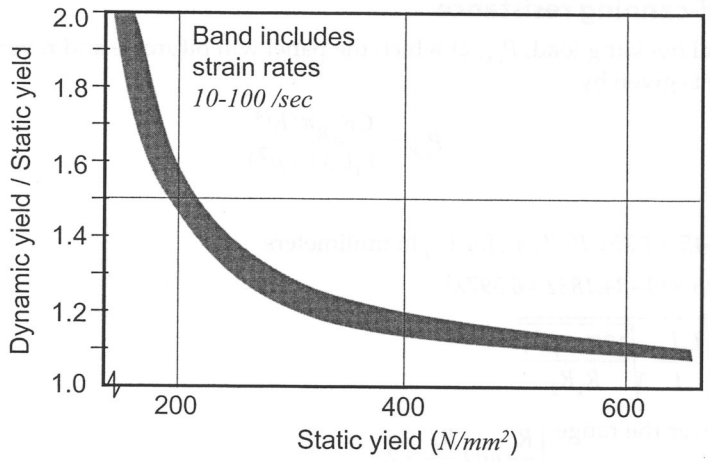

Figure 3.95 Dynamic yield stress for steel.

Example: Curved panel behavior

A steel automobile hood outer panel is shown in Figure 3.96. A portion of the panel, with the given dimensions, is supported at its periphery by the hood inner structure, which provides simply supported boundary conditions. The dynamic yield stress is σ_{YD}=298 N/mm². What is the panel stiffness, oil-can load, and denting energy?

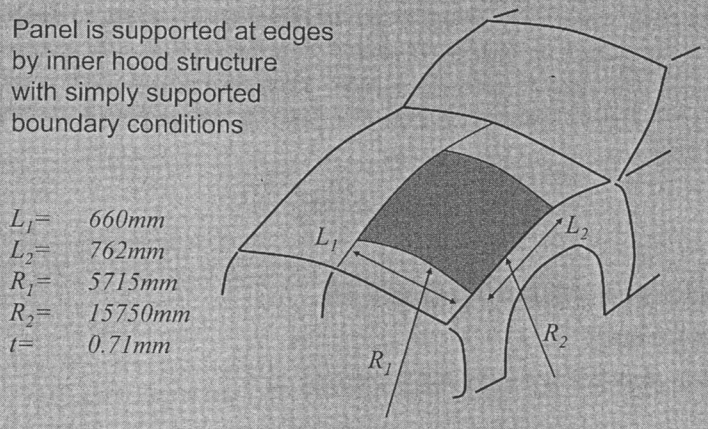

Figure 3.96 Automobile hood panel.

To determine stiffness, we will use Equation 3.35, but first need the panel crown height, H_C, given below Equation 3.37a,

$$H_C = \left(\frac{(660mm)^2}{8(5715mm)}\right) + \left(\frac{(762mm)^2}{8(15750mm)}\right) = 14.14mm$$

Now using Equation 3.37b to arrive at the equivalent spherical curvature for the panel:

$$\frac{1}{R_{EQ}} = \frac{4(14.14mm)}{(660mm)(762mm)} = 0.0001124/mm$$

Finally using Equation 3.35 with $B=2.309$:

$$K = 2.309(0.00011246/mm)\frac{(207000N/mm^2)(0.71mm)^2}{\sqrt{1-0.3^2}} = 28.39N/mm$$

Oil can load is given by Equation 3.38, where:

$$C = 0.645 - 7.75 \times 10^{-7}(660mm)(762mm) = 0.255$$

$$\lambda = .5\sqrt{\frac{660mm \cdot 762mm}{0.71mm}}\sqrt{\frac{12(1-0.3^2)}{5715mm \cdot 15750mm}} = 7.854$$

$$R_{CR} = 45.929 - 34.183\lambda + 6.397\lambda^2 = 172$$

Then substituting into Equation 3.38:

$$P_{CR} = \frac{(.255)(172)\pi^2(207000N/mm^2)(0.71mm)^4}{660mm \cdot 762mm(1-0.3^2)} = 50N$$

The denting energy is given by Equation 3.39 where we have calculated the panel stiffness, K, above:

$$W = 56.8\frac{(298N/mm^2(0.71mm)^2)^2}{28.39N/mm}$$

$$W = 4.515 \times 10^4 Nmm$$

3.6.5 In-plane loading of panels

In this section we will look at panels where the applied loads are within the plane of the panel, Figure 3.93. This includes membrane panels which are curved, but over a small element of the surface, the loads are tangent to the surface. A second case of in-plane loading—that of shear loading of panels—will be treated later in the chapter on body torsion.

3.6.5.1 Membrane shaped panels

Many of the structural elements of the underbody are panels, including floor pan, motor compartment sides, dash, and wheelhouse inner panel. Unlike the exterior panels, these underbody panels are largely shaped by structural requirements. Therefore, our orientation in this section is that of design rather than analysis. The question we would like to answer is: Given a set of loads applied to a panel, what is the best panel shape to react to those loads? (*Best* here is defined as stiffest, strongest, and lightest.) We begin with a simple observation: consider a small element taken from a loaded panel and viewed from its edge, Figure 3.97. If the loading on the panel is pure bending, the stress distribution is linear with zero stress at the neutral axis, Figure 3.97a. Intuitively, much of the material of the section is stressed at a relatively low level yet we are 'paying' for the mass of that material.

The panel stiffness in bending, $D = \frac{Et^3}{12(1-\mu^2)}$, is very low since the thickness in

automotive panels is very small. Now consider a panel loaded by pure membrane loads, Figure 3.97b. All the material of the section is uniformly stressed across the thickness and contributes to reacting the applied load. Given this fully stressed quality of a membrane, we would like to design the panel *shape* such that only membrane loading is present.

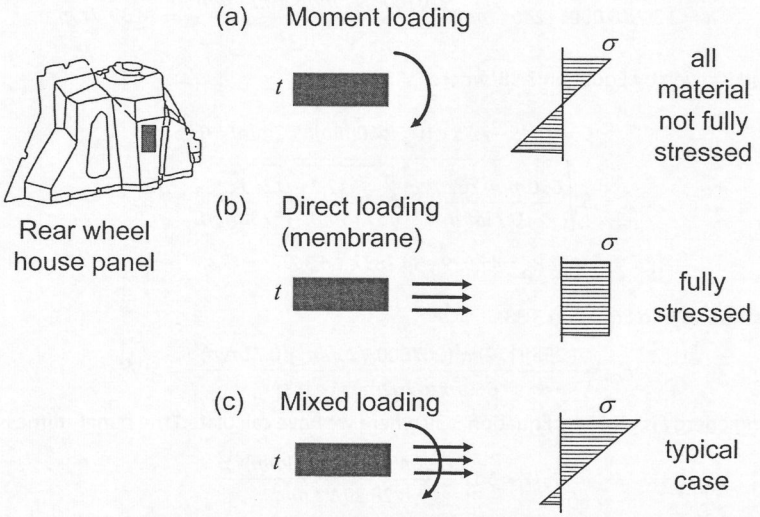

Figure 3.97 Element from loaded panel.

For simplicity in understanding basic structural behavior, we will consider axially symmetrical membranes, Figure 3.98. The membrane surface is defined by rotating a *generating line* about the axis of symmetry. Consider a small element on the surface. Two radii of curvature define the geometry of the element. A longitudinal radius, R_L,

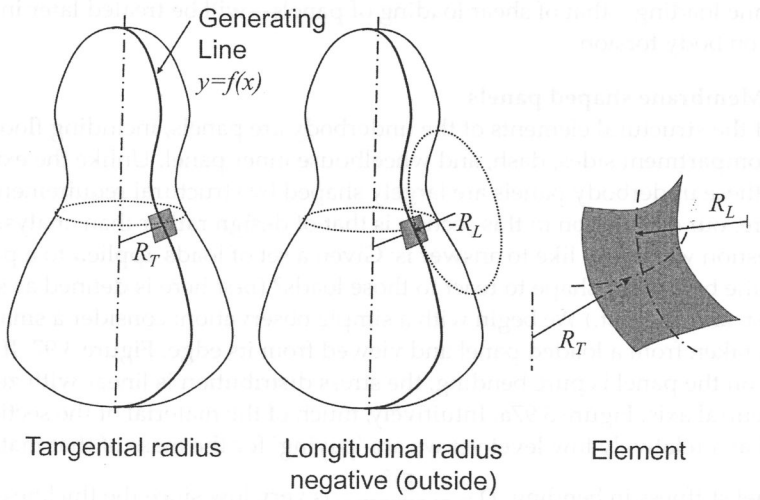

Figure 3.98 Axially symmetric membrane geometry.

which defines the radius of a longitudinal section of the element, and a tangential radius, R_T, which defines the radius of a tangential section of the element. The longitudinal radius is defined by the curvature of the generating line at the point where the element sits. The tangential radius is a line which is normal to the element and extends to the axis of the membrane.

Acting on the element are tangential stresses, σ_{TAN}, and longitudinal stresses, σ_{LONG}, as shown in Figure 3.99, as well as an outward pressure, p. These stresses are uniform across the thickness. The element must be in static equilibrium, and balancing forces in the direction normal to the element, Figure, 3.99:

$$p(ds)(ds') - 2\sigma_{TAN}(tds')\frac{d\theta}{2} + 2\sigma_{LONG}(tds)\frac{d\phi}{2} = 0$$

from geometry, $ds'=R_T\, d\theta$ and $ds=R_L\, d\phi$, and substituting into the above yields the first equation a membrane surface must satisfy:

$$\frac{p}{t} = \frac{\sigma_{TAN}}{R_T} + \frac{\sigma_{LONG}}{R_L} \tag{3.40}$$

where:

p = Pressure normal to membrane

t = Thickness of membrane

σ_{TAN} = Tangential stress

σ_{LONG} = Longitudinal stress

R_T = Radius of curvature in tangential direction

R_L = Radius of curvature in longitudinal direction

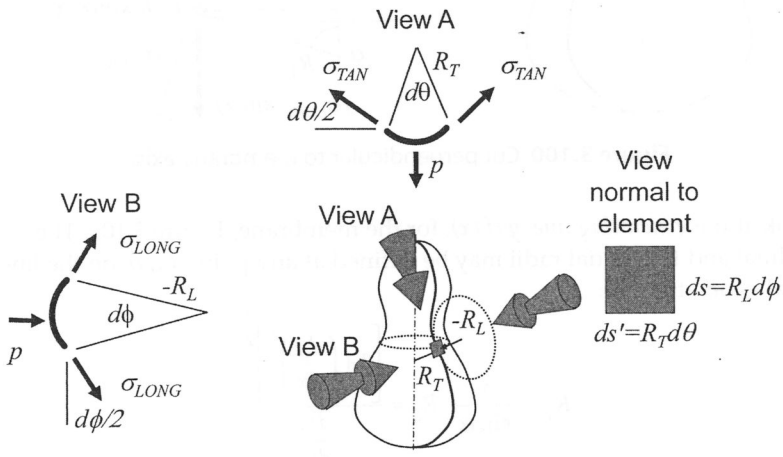

Figure 3.99 Loads on membrane element.

Now cutting the membrane perpendicular to the axis, Figure 3.100, the cut portion may be placed into equilibrium in the axial direction. The net upward force on the cut section is F, and along the cut the longitudinal stress, σ_{LONG}, acts. At the cut, the

normal to the surface makes an angle α with the axis as shown. Static equilibrium yields the second equation a membrane surface must satisfy:

F=(component of stress along axis)/(Area on which stress acts)

$$F = (\sigma_{LONG} \sin\alpha)(2\pi\, t\, x) \text{ or } F = (\sigma_{LONG} \sin\alpha)(2\pi\, t\, R_T \sin\alpha)$$

$$F = 2\pi\, t\, x(\sigma_{LONG} \sin\alpha) \text{ or } F = 2\pi\, t\, R_T \sigma_{LONG} \sin^2\alpha \tag{3.41}$$

where:

F = Net force acting on a cut portion of membrane

α = Angle made between normal to the surface with the axis

t = Thickness of membrane

σ_{LONG} = Longitudinal stress

R_T = Radius of curvature in tangential direction

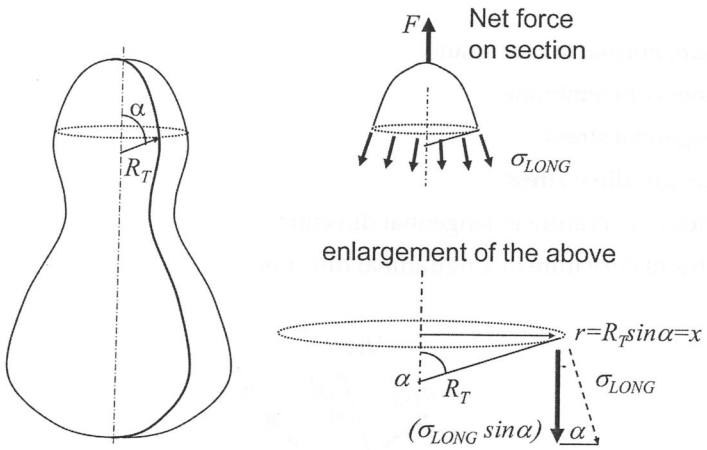

Figure 3.100 Cut perpendicular to membrane axis.

Now look at the *generating line, y=f(x)*, for the membrane, Figure 3.101. The longitudinal and tangential radii may be defined at any point, *(x,y)*, on the line using analytical geometry [20]:

$$R_T = \frac{x}{\sin\alpha},\ R_L = \frac{\left[1+\left(\frac{dy}{dx}\right)^2\right]^{\frac{3}{2}}}{\frac{d^2y}{dx^2}}$$

$$\sin(\alpha) = \frac{\frac{dy}{dx}}{\left[1+\left(\frac{dy}{dx}\right)^2\right]^{\frac{1}{2}}},\ \cos(\alpha) = \frac{1}{\left[1+\left(\frac{dy}{dx}\right)^2\right]^{\frac{1}{2}}} \tag{3.42}$$

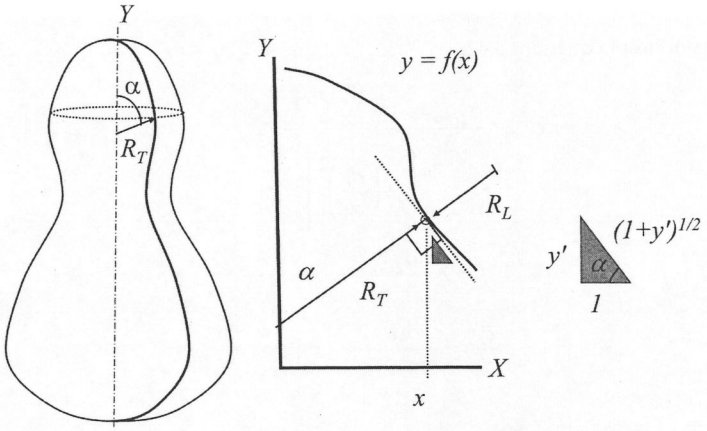

Figure 3.101 Membrane generating line.

With the set of Equations 3.40, 3.41, and 3.42 we can now determine *the* membrane shape, defined by the generating line, $y=f(x)$, for a specific loading. The sequence we will follow is:

1. Define the loading
2. Substitute the loading into the force balance, Equation 3.41
3. Substitute into the resulting equation the geometric relationships of Equations 3.42
4. A differential equation for the generating line will result, which we solve for $y=f(x)$ to define the shape of the membrane panel.

Example: Uniform load on circular membrane

Consider a panel with a uniform pressure load of p and a circular boundary. Such a load may represent an automobile rear compartment load floor. What is the shape of a panel which will react this loading with only membrane stress?

The total load $F= p(Area)=p\pi x^2$ substituting into Equation 3.41

$$p\pi x^2 = 2\pi\, t\, x(\sigma_{LONG} \sin\alpha)$$

and substituting for $\sin\alpha$ from Equations 3.42:

$$x = 2t\frac{\sigma_{LONG}}{p}\frac{\frac{dy}{dx}}{\left[1+\left(\frac{dy}{dx}\right)^2\right]^{\frac{1}{2}}}$$

$$\beta = 2t\frac{\sigma_{LONG}}{p}$$

$$\frac{dy}{dx} = \frac{x}{\left[\beta^2 - x^2\right]^{\frac{1}{2}}}$$

$$y = \int \frac{x}{\left[\beta^2 - x^2\right]^{\frac{1}{2}}} dx$$

which may be integrated to determine the generating line resulting in:

$$x^2 + y^2 = \beta^2,\ \beta = 2t\frac{\sigma_{LONG}}{p} \tag{3.43}$$

which gives a circle of radius β as a generating line, and when swept about an axis, gives a spherical surface as the panel shape with $R_T = \beta$ and $R_L = \beta$. Substituting the value for β into Equation 3.40:

$$\frac{p}{t} = \frac{\sigma_{TAN}}{\left(2t\frac{\sigma_{LONG}}{p}\right)} + \frac{\sigma_{LONG}}{\left(2t\frac{\sigma_{LONG}}{p}\right)}$$

$$\sigma_{TAN} = \sigma_{LONG} = \frac{p\beta}{2t} \tag{3.44}$$

So as designers of the panel loaded as above, if we shape the panel as a spherical surface, the loaded panel will have no bending stress and will have a uniform design stress across the thickness given by $\sigma = p\beta/2t$. As the material is fully stressed, the panel will be stiffer than alternative shapes.

Example: Circular membrane loaded by rigid ring

Consider a panel with a load, *F*, applied to a rigid ring, Figure 3.102a. Again the boundary of the panel is circular. Such a panel is an idealization of a suspension attachment point. What is the shape of a panel which will react this loading with only membrane stress?

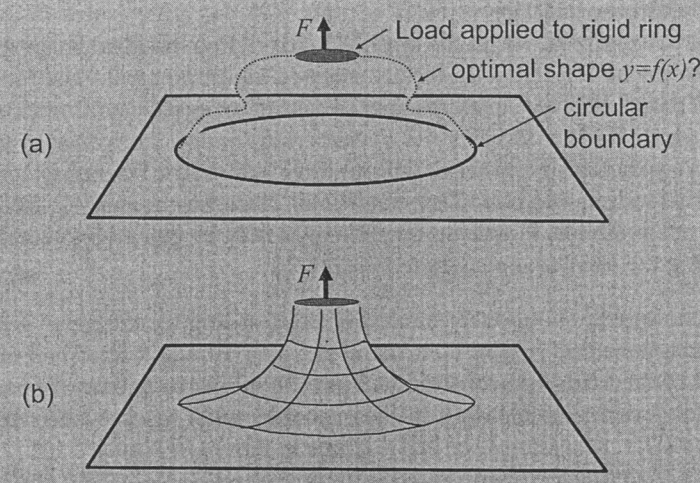

Figure 3.102 Circular membrane loaded by rigid ring.

Equation 3.41 gives:

$$F = (2\pi x) t \sigma_{LONG} \sin\alpha$$

$$F = 2\pi t \sigma_{LONG} \frac{x\frac{dy}{dx}}{\left[1+\left(\frac{dy}{dx}\right)^2\right]^{\frac{1}{2}}}$$

$$\text{letting } \rho = \frac{F}{2\pi t \sigma_{LONG}}$$

$$\frac{y}{\rho} = \int \frac{1}{\left[\left(\frac{x}{\rho}\right)^2 - 1\right]^{\frac{1}{2}}} d\left(\frac{x}{\rho}\right)$$

$$\frac{x}{\rho} = \cosh\left(\frac{y}{\rho}\right) \tag{3.45}$$

which gives a horn-shaped surface as the panel shape. From Equation 3.40 we find

$$R_T = R_L \tag{3.46}$$

and each element on the surface is a saddle shape as in the patch shown in Figure 3.98. Again both stresses are equal:

$$\sigma_{TAN} = \sigma_{LONG} = \frac{F}{2\pi t \rho} \tag{3.47}$$

As the designer of this panel, we shape the panel into the horn shape described by Equation 3.45 and the loaded panel will have no bending stress, and we expect the panel to be stiffer than alternative shapes.

3.6.5.2 Membrane analogy

In the above examples, we let the applied loads define the ideal shape for the panel with the notion that a uniformly stressed membrane panel will result in a light, stiff panel. We have used the special case of an axially symmetric membrane to demonstrate basic principles and to ease computation. However, rarely in automotive panel design practice will we have symmetric boundary conditions. For general loading and boundary conditions, closed-form analytic solutions are typically not available. However, much insight may be gained by visualizing panel shape using the *membrane analogy technique* [21].

In this technique the boundary constraints and loading for the panel are accepted, and we imagine a thin rubber membrane or a soap film [22] stretched under the action of the loads and constraints. Both the rubber membrane or soap film are structures with zero bending stiffness, so they must react to loads in a pure membrane state. An example of this analogy is shown in Figure 3.103 [23]. Here the objective is to define the shape for a building roof when loaded by uniform dead weight. A model of the roof is visualized using a membrane analogy—a light fabric cloth saturated with plaster. The desired four restraints are applied at the corners, and the weight of the plaster provides the uniform downward load on the inverted structure. The shape taken by the fabric is that of a membrane having uniform stress (no bending) across the structure's thickness.

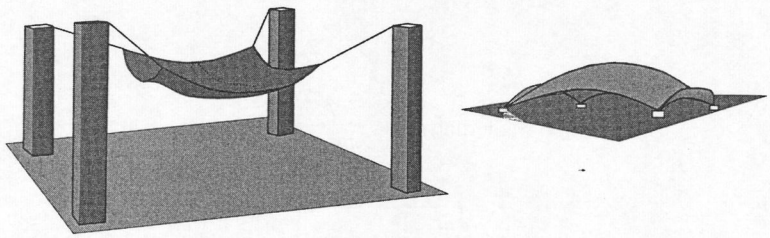

Figure 3.103 Membrane shaped roof structure.

Example: Rear load floor panel

Vibration of the rear load floor panel is a source of noise in the automobile. Generally a high resonance frequency for the panel is desirable, and this implies a high normal stiffness. The inertial loads during vibration approximate a uniformly distributed normal load across the panel. To maximize panel stiffness in this condition, we would like to define the membrane shape for a uniform downward load satisfying the irregular panel boundary, Figure 3.104a.

A heated plastic film was constrained at the boundary and loaded by its weight, simulating the uniformly distributed load. In the heated state, the film had only the ability to generate direct stress and behaved as a membrane. Upon cooling, the film held its shape, shown in Figure 3.104b. The shape is similar to the spherical membrane in *Example 2* above, but accommodates the irregular boundary conditions.

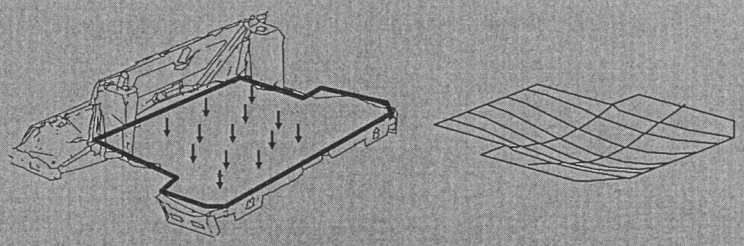

Distributed load and boundary (a)

Membrane shaped rear panel (b)

Figure 3.104 Membrane shaped panel for rear load floor.

Example: Suspension strut attachment panel

The suspension strut loads are often reacted by the wheelhouse panel. These strut loads are point loads directed along the axis of the strut. Figure 3.105a shows a typical strut attachment for the front suspension and Figure 3.105b for the rear suspension. The boundary restraints for the wheelhouse panels are generally irregular and non-planar, Figure 3.106a & b. High panel stiffness at the point of load attachment is desirable, and we would like to determine a membrane shape under these loads which satisfy the irregular boundary conditions.

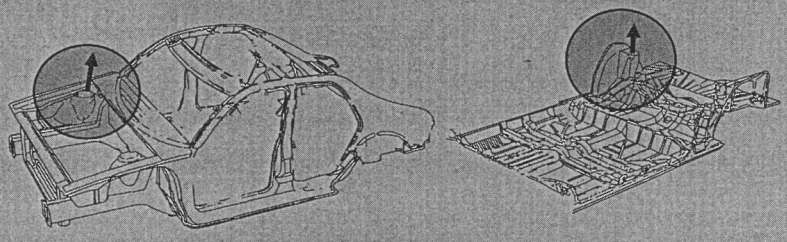

Front suspension (a)

Rear suspension (b)

Figure 3.105 Suspension strut attachment panels.

Using the same technique as used in example 1 above, a heated plastic film was constrained at the boundary and loaded in the direction of the strut axis through a small rigid disk representing the strut mounting bracket. For the motor compartment panel, Figure 3.107 shows the rigid boundary, the unloaded membrane, and finally the resulting loaded membrane shape. Figure 3.108 shows the rear panel membrane shape. Note the similarity to the horn membrane shape in the earlier axis-symmetrical example, Figure 102, but now accommodating the irregular boundary conditions. Note also that any small element on this panel also has a saddle shape, which is required by Equation 3.40 whenever the distributed load p is zero.

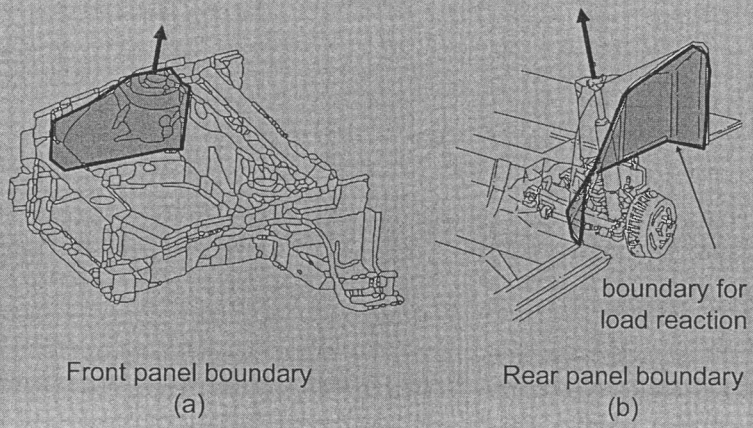

Figure 3.106 Boundaries for strut attachment panels.

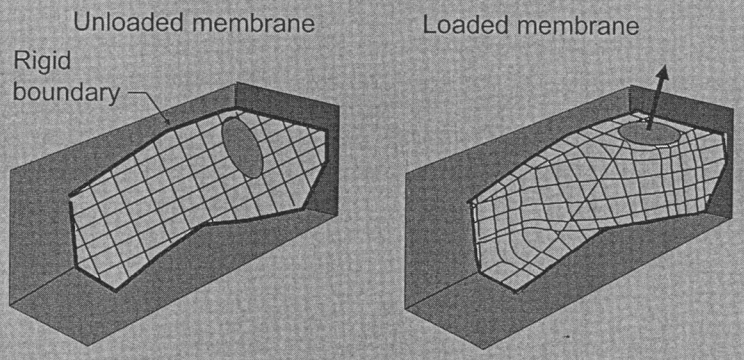

Figure 3.107 Forming motor compartment panel as a membrane.

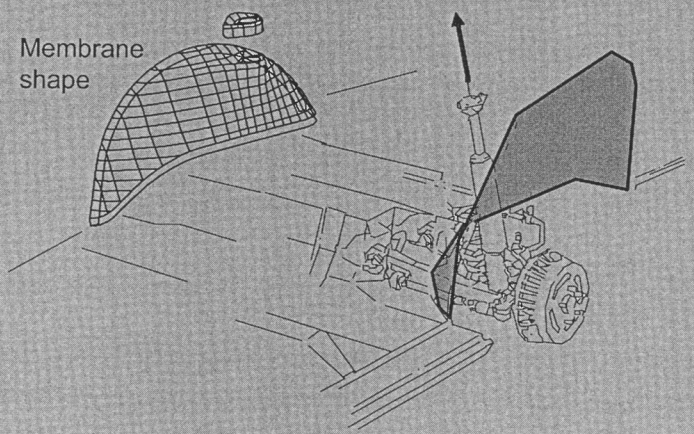

Figure 3.108 Rear strut attachment-membrane wheel house.

Once a panel has this more efficient membrane shape, the predominant internal loads act tangent to the surface at any point. In restraining such a panel, the weld flanges must also be tangent to the surface and the panel must blend smoothly into the supporting boundary structure to realize the stiffness offered by the membrane shape, Figure 3.109.

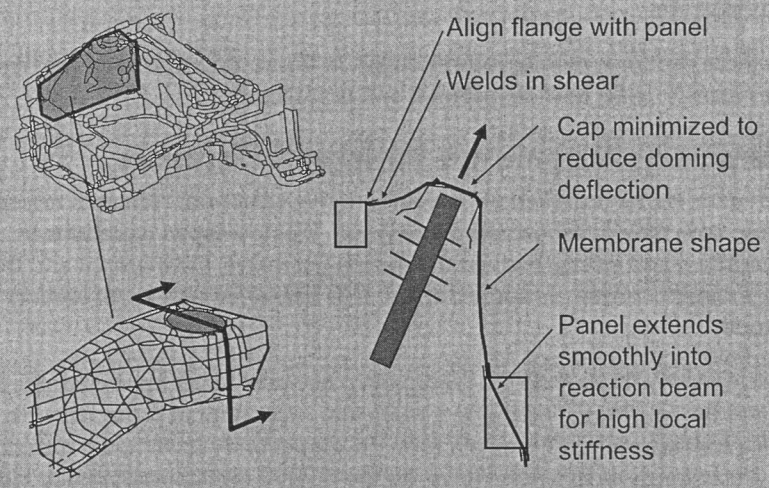

Figure 3.109 Reacting tensile loads in a membrane panel.

Modeling sheet metal structures as ideal membranes is certainly an approximation. Comparing some attributes between actual sheet metal and ideal membrane behavior:

Idealized Membrane Behavior: Can accept either tensile or compressive stress

Actual Sheet Metal Behavior: Buckling can occur under compressive stress

This is a serious limitation to the practical application of membrane panels. Proper design must seek to generate tensile loads only, or assure the buckling stress will not be exceeded. In the case of load floors or strut towers, tensile stresses are assured due to the unidirectional nature of the load.

Idealized Membrane Behavior: All stress lies in plane of surface (direct stress only)

Actual Sheet Metal Behavior: Bending stresses can be reacted

This is a highly beneficial property of real panels. Because membrane geometry can balance only the set of loads used to define it, the panel should collapse when the load deviates even slightly as it does in practice. That this does not occur is due to the ability to generate bending moments in the real panel.

Idealized Membrane Behavior: Boundary conditions are ideal (boundary loads are tangent to surface)

Actual Sheet Metal Behavior: Boundary conditions do not agree completely with theoretical requirements

This provides a general design constraint on the geometry of the structure at the boundary of a membrane panel. The required tangent reactions can practically be achieved only imperfectly and require bending moments to be generated in the reaction structure.

Despite these cautions, membrane structures in the automotive body are highly efficient means to react both distributed and point loads.

3.7 Summary: Automotive Structural Elements

In this chapter we have looked at how automotive structural elements respond to loading, how they deflect, and how they fail. We developed equations to predict stiffness and strength given the section geometry, the material and the bending moment, torque, or applied force. This has given us a set of section design tools.

However, to apply these tools the relationship between loads applied to the body system and the resulting loading on a particular section must be known. We need to *flow down* structural requirements from the global body level to the individual section. An example of this flow down for the B Pillar section is shown in Figure 3.110. In the subsequent chapters we will look at this flow down of requirements for several global body system cases including body bending, body torsion, crashworthiness, and vibration.

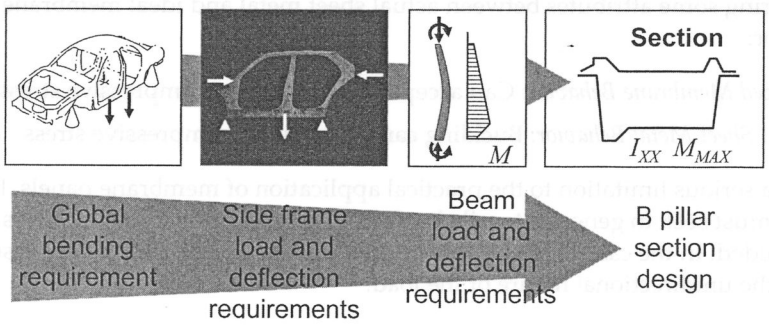

Figure 3.110 Flow of body strength and stiffness requirements.

References

1. Byars, E. and Snyder, R., *Engineering Mechanics of Deformable Bodies*, International Textbook Co, Scranton, PA, 1964.
2. "Geometrical Analysis of Sections," CARS 2008 Software, Amerian Iron and Steel Institute, Southfield, MI, 2008.
3. Den Hartog, J. P., *Advanced Strength of Materials*, McGraw-Hill Co, NY, 1952.
4. Crandall, S., Dahl, N. and Lardner, T., *An Introduction to the Mechanics of Solids*, McGraw-Hill, NY, 1978.
5. Timoshenko, S. and Goodier, J., *Theory of Elasticity*, McGraw-Hill Co., NY, 1951.
6. Roark, R. and Young, W., *Formulas for Stress and Strain*, McGraw-Hill Co., NY, 1982.
7. Nisawa, J., Tomioka, N. and Yi, W., "Analytical Method of Rigidities of Thin Walled Beams with Spot Welding Joints and Its Application to Torsion Problems," JSAE Review, March 1985, pp. 76–83.
8. Kikuchi, N. & Malen, D., Course notes for ME513 Fundamentals of Body Engineering, University of Michigan, Ann Arbor, MI, 2007.
9. Timoshenko S., *Theory of Plates and Shells*, McGraw Hill, NY, 1959. pp. 444–447.
10. Timoshenko, S. and Gere, J., *Theory of Elastic Stability*, McGraw Hill, NY, 1961.
11. Yu, Wei-Wen, *Cold-Formed Steel Design*, John Wiley & Sons, NY, 1985.
12. Bloom, F. and Coffin, D., *Handbook of Thin Plate Buckling and Postbuckling*, Chapman & Hall/CRC, NY, 2001.
13. *Aluminum Construction Manual, Section 1-Specification for Aluminum Structures*, Aluminum Association, Washington, DC, 1970.
14. Cook, R. and Young, W., *Advanced Mechanics of Materials*, Macmillan Co., NY, 1985.
15. Lin, Kuang-Huei, "Stiffness and Strength of Square Thin-Walled Beams," SAE Paper No. 840734, SAE International, Warrendale, PA, 1984.
16. Parks, M. B. and Yu, W. W., "Structural Behavior of Members Consisting of Flat and Curved Elements," SAE Paper No. 870464, SAE International, Warrendale, PA, 1987.
17. Bruhn, E. F., *Analysis & Design of Flight Vehicle Structures*, Tri-State Offset Co., USA, 1973.
18. *Cold-Formed Steel Design Manual*, American Iron and Steel Institute, Washington, DC, 1986, Section 3.3.4.
19. Swenson, W. E. and Traficante, R.J., "The Influence of Aluminum Properties on the Design, Manufacturability and Economics of an Automotive Body Panel," SAE Paper No. 820385, SAE International, Warrendale, PA, 1985.
20. Goodman, A. W., *Analytic Geometry and the Calculus*, Mac Millan Co, NY 1963, pp. 269, 292.

21. Malen, D. E., *Empirical Method for Determining the Shape of a Vehicle Body Membrane Panel*, US Patent 4,581, 192, April 8, 1986.

22. Kato, T., Hoshi, K. and Umemura, E., "Application of Soap Film Geometry for Low Noise Floor Panels," *Proceedings of the 1999 Noise and Vibration Conference*, P-342, SAE 1999-01-1799, SAE International, Warrendale, PA, 1999.

23. Billington, D., *Heinz Isler as Structural Artist*, Catalog for exposition at Princeton University, April 1980.